Resonance Enhancement with Antenna Modeling

Kristensson, Gerhard; Cheney, Margaret; Kim, Jerry

2018

Document Version:
Publisher's PDF, also known as Version of record

CODEN:LUTEDX/(TEAT-7261)/1-28/(2018)
Revision No. 1: February 2022

Resonance Enhancement with Antenna Modeling

Gerhard Kristensson, Margaret Cheney, and Jerry Kim

Electromagnetic Theory
Department of Electrical and Information Technology
Lund University
Sweden

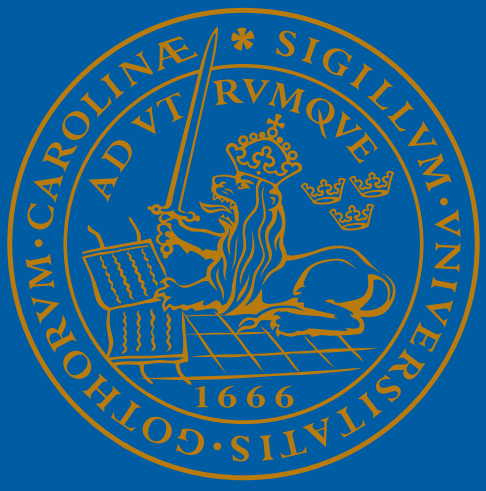

(TEAT-7261)/1-28/(2018): G. Kristensson, M. Cheney, and J. Kim, Resonance Enhancement with Antenna Modeling

Gerhard Kristensson
gerhard.kristensson@eit.lth.se

Department of Electrical and Information Technology
Electromagnetics and Nanoelectronics
Lund University
P.O. Box 118
SE-221 00 Lund
Sweden

Margaret Cheney
cheney@math.colostate.edu

Department of Mathematics and
Department Electrical and Computer Engineering
Colorado State University
1874 Campus Delivery
Fort Collins, CO 80523
USA

Jerry Kim
jerry.t.kim.ctr@us.navy.mil

Office of Naval Research
875 Randolph Street
Arlington, VA 22203
USA

Editor: Mats Gustafsson

Abstract

This paper develops theory for an iterative experimental approach to use one or more antennas to identify resonances of a scattering system, which could consist of the antennas and one or more scattering objects. We include realistic mathematical models for the antennas and for target(s), and we show that the resonances include effects from the antennas and wave propagation as well as the target scattering operator and its poles. We show how the effects of the antennas and wave propagation paths can be removed, to leave only the effect of the target scattering operator. We include simulations for the case of one and two cylindrical dipole antennas probing a dielectric sphere, and we show the effect of antenna resonances on the iterative experimental process.

1 Introduction

For remote target identification, one of the challenges is that targets look different from different viewing aspects. Consequently there has long been interest in making use of target features that are independent of viewing aspect [19,25]; one class of such features are target resonances. A promising approach, the Singularity Expansion Method (SEM) was proposed by Baum [2,3], in which he noted that each target has a scattering operator that has certain poles in the complex plane [14]. These poles do not depend on the viewing angle, but the challenge is to find a way to extract the poles from time-domain scattering data [30, 32, 34, 35].

An independent line of investigation determined the time-domain waveform that returns the most scattered energy from a target [10, 22]. In general, the best waveform is a single-frequency waveform whose frequency can be found experimentally by an iterative process in which each successive backscattered signal is time-reversed and retransmitted.

The fact that the solution to this problem involves an iterative time-reversal process thus makes a connection with a long line of work on time reversal, including [4,16] and references in [16]. Much of this work addresses different types of problems, such as refocusing on a source through an inhomogeneous medium. Other previous work addresses the connection between eigenvalues of the time-reversal operator and target characteristics [6–9,38]. To distinguish our use of iterative time-reversal from other types of problems whose solutions also involve a time-reversal process, we refer to our approach as the Resonance Enhancement Method (REM).

REM has been used experimentally to identify acoustic target resonances from a single-channel system [28,39]. The paper [26] carried out two-channel simulations for idealized antennas and targets, and suggested a possible connection with Baum's SEM method.

In this paper we extend the work of [26] to the case of more accurate modeling of antenna and target behavior. In particular, we address the issue of how the antenna affects our ability to obtain information about the target frequency response. In a subsequent paper we investigate the connection between this approach and the SEM method.

This work focuses on the case of one or more antennas, which could be spatially distributed, and a target, which could consist of multiple scattering objects, embedded in free space. We assume that the target is located in the far zone of each antenna, and each antenna is located in the far zone of the scatterer. However, the scatterer does not need to be in the far zone of the entire antenna configuration, only in the far zone of each antenna.

We emphasize that the experiments are done in time domain; however much of the analysis is carried out in the frequency domain for convenience.

2 Antenna description

The antennas used in this paper act both as a transmitting and a receiving device. The generic geometry of a typical antenna is depicted in Figure 1, where the radiating part is colored red, and the supporting electronics with the detector/generator (in green) is colored blue. The surrounding medium is assumed to be homogeneous, lossless, and isotropic, characterized by the relative permittivity $\epsilon(k)$ and the permeability $\mu(k)$. Here, $k = \omega/c$ is the wave number of the exterior medium, ω is the angular frequency, and c is the light speed. The assumption of a lossless surrounding material implies that $\epsilon(k)$ and $\mu(k)$ are real-valued numbers.[1]

A transmission line feeds the antenna. The fields in a transmission line can be characterized either by the voltage $V(k)$ and the current $I(k)$, or, equivalently, by the amplitudes, $\alpha(k)$ and $\beta(k)$, of the two traveling waves. The quantities are monitored at a fixed position (the reference plane), and the spatial behavior is irrelevant for us in this paper, and therefore suppressed. For our needs, it is advantageous to use the amplitudes of the two traveling waves on the feed.

The wave that propagates to the right (from the signal generator to the antenna) has amplitude $\alpha(k)$, and the one that propagates to the left (output from the antenna, which enters the detector) has amplitude $\beta(k)$; see Figure 1. The (possibly complex-valued) amplitudes $\alpha(k)$ and $\beta(k)$, which both have dimensions of Volts (V), act like input and output, respectively, to the antenna configuration. In terms of the voltage $V(k)$ and current $I(k)$ on the transmission line, the amplitudes of the waves are defined by

$$\alpha(k) = \frac{1}{2}\left(V(k) + Z(k)I(k)\right), \qquad \beta(k) = \frac{1}{2}\left(V(k) - Z(k)I(k)\right)$$

with inverse

$$V(k) = \alpha(k) + \beta(k), \qquad Z(k)I(k) = \alpha(k) - \beta(k)$$

where the transmission line characteristic impedance $Z(k) = \sqrt{\mu_0\mu(k)/\epsilon_0\epsilon(k)}$ is a positive, real-valued function of k. Note that the characteristic impedance is the same for all transmission lines, and it is generally frequency-independent.

In the surrounding space, there are two vectors that characterize the interaction with the antenna, *viz.*, the far field amplitude of the antenna in the far field zone,

[1] We allow for a dependence on the wave number k (or frequency), which can be used to model existing dispersion effects.

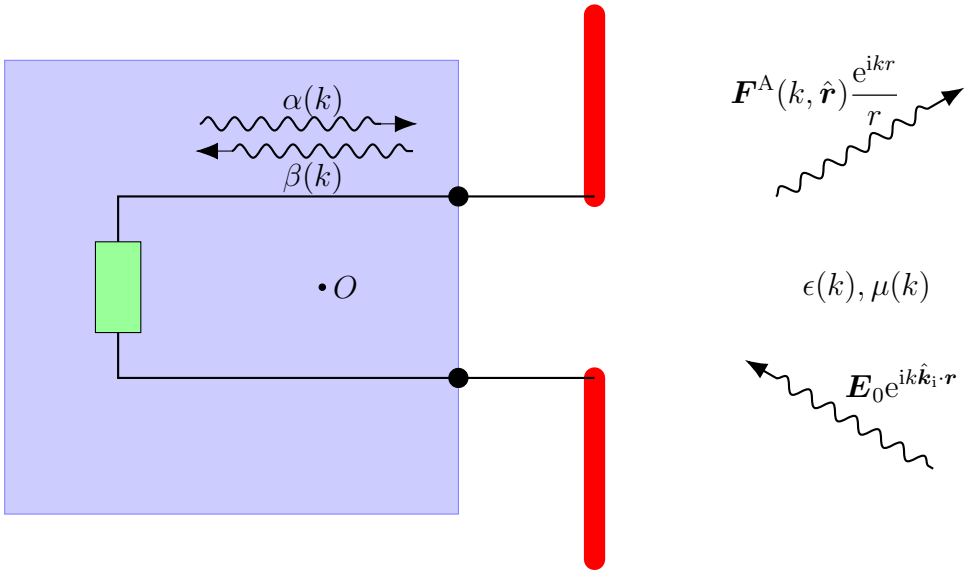

Figure 1: The generic geometry of an antenna (red), the supporting electronics with the detector (blue), and its exciting amplitude $\alpha(k)$ and the field $\boldsymbol{E}_0$. The detector/generator is marked with a green box. The reference point (local origin) is denoted O. The outputs are the amplitude $\beta(k)$ and the far field amplitude $\boldsymbol{F}^{\mathrm{A}}(k,\hat{\boldsymbol{r}})$.

$\boldsymbol{F}^{\mathrm{A}}(k,\hat{\boldsymbol{r}})$, and the receiving electric field, $\boldsymbol{E}_0(k)$, at the reference point of the antenna (usually taken as the local origin O; see Figure 1).

If the antenna acts as a transmitter, we have an excitation of the system from the generator in the shielded electronics of the antenna. This excitation is quantified by coefficient $\alpha(k)$. This excitation generates an electromagnetic field outside the antenna, which in the direction $\hat{\boldsymbol{r}}$ in the far field zone is quantified by the far field amplitude $\boldsymbol{F}^{\mathrm{A}}(k,\hat{\boldsymbol{r}})$. The electric field in the far zone is [29]

$$\boldsymbol{E}(k,\boldsymbol{r}) \approx \boldsymbol{F}^{\mathrm{A}}(k,\hat{\boldsymbol{r}})\frac{\mathrm{e}^{\mathrm{i}kr}}{r} \tag{2.1}$$

The far field amplitude depends linearly on the coefficient $\alpha(k)$, and we formally write the relation between the far field amplitude of the antenna and the excitation $\alpha(k)$ as

$$\boldsymbol{F}^{\mathrm{A}}(k,\hat{\boldsymbol{r}}) = \boldsymbol{f}(k,\hat{\boldsymbol{r}})\alpha(k) \tag{2.2}$$

which defines the dimensionless vector $\boldsymbol{f}(k,\hat{\boldsymbol{r}}) \in \mathbb{C}^3$. Because the far-field electric field is perpendicular to the direction of propagation, the vectors $\boldsymbol{F}^{\mathrm{A}}(k,\hat{\boldsymbol{r}})$ and $\boldsymbol{f}(k,\hat{\boldsymbol{r}})$ are restricted to the plane perpendicular to $\hat{\boldsymbol{r}}$; in other words, the vector $\boldsymbol{f}(k,\hat{\boldsymbol{r}})$ can be thought of as being in the (complex) tangent space at $\hat{\boldsymbol{r}}$ to the unit sphere.

In receiving mode, the excitation of the antenna is made by an incident plane wave (see Figure 1)

$$\boldsymbol{E}_0(k)\mathrm{e}^{\mathrm{i}k\hat{\boldsymbol{k}}_{\mathrm{i}}\cdot\boldsymbol{r}}$$

where k is the wave number of the surrounding material, the unit vector $\hat{\boldsymbol{k}}_{\mathrm{i}}$ denotes the direction of the plane wave, and the constant, complex vector $\boldsymbol{E}_0(k)$ denotes the exciting field at the origin. This excitation generates a traveling wave in the port, which is quantified by the coefficient $\beta(k)$. Due to linearity of the antenna system, the connection between $\boldsymbol{E}_0$ and $\beta(k)$ can be written as [11, 17, 21, 27]

$$\beta(k) = \frac{2\pi\mathrm{i}}{k}\boldsymbol{s}(k, \hat{\boldsymbol{k}}_{\mathrm{i}}) \cdot \boldsymbol{E}_0(k) \tag{2.3}$$

for some dimensionless vector field $\boldsymbol{s}(k, \hat{\boldsymbol{k}}_{\mathrm{i}})$. The extra factor $2\pi\mathrm{i}/k$ is included so that a reciprocal antenna has the property $\boldsymbol{s}(k, \hat{\boldsymbol{r}}) = \boldsymbol{f}(k, -\hat{\boldsymbol{r}})$ [12, 18, 33, 36].

The relation (2.3) is not a complete description of a receiving antenna. In general, there are two more contributions to the system. First, there is a term that quantifies the reflection of the received traveling wave in the transmission line by the electronics. With the assumption of the load matched to the transmission line (which can almost always be arranged), this term vanishes. Moreover, there is a scattering contribution generated by the incident plane wave. This term is usually appreciable, but we can ignore this contribution in this paper, as we amplify the re-radiated, time reversed signal $\alpha(k)$ (the scalar A below). Thus, the scattered contribution is negligible compared to this re-radiated signal, and the scattered contribution can be ignored.

For a reciprocal antenna $\boldsymbol{s}(k, \hat{\boldsymbol{r}}) = \boldsymbol{f}(k, -\hat{\boldsymbol{r}})$, and the receiving case is

$$\beta(k) = \frac{2\pi\mathrm{i}}{k}\boldsymbol{f}(k, -\hat{\boldsymbol{k}}_{\mathrm{i}}) \cdot \boldsymbol{E}_0(k) \tag{2.4}$$

Under these assumptions, the antenna, both in transmitting and receiving mode, is characterized by a single complex vector field $\boldsymbol{f}(k, \hat{\boldsymbol{r}})$. The variation of this vector field with frequency and direction can complicate our efforts to obtain target information.

2.1 Antenna example

A center-fed, cylindrical dipole antenna of length 2ℓ and radius d illustrates the antenna characterization above. This antenna has an approximate far field amplitude [15]

$$\boldsymbol{F}^{\mathrm{A}}(k, \hat{\boldsymbol{r}}) = -\frac{\mathrm{i}Z(k)I_0(k)}{2\pi}\frac{\cos(k\ell\cos\vartheta) - \cos(k\ell)}{\sin\vartheta}\hat{\boldsymbol{\vartheta}}$$

where $I_0(k)$ is the amplitude of the current at the antenna feed and ϑ is the angle between the extension of the linear antenna (z axis) and the observation direction $\hat{\boldsymbol{r}}$; see the inset in Figure 2. This current $I_0(k)$ and the voltage $V_0(k)$ at the feed are related to the antenna impedance $Z_{\mathrm{in}}(k)$ and the amplitudes $\alpha(k)$ and $\beta(k)$ via

$$\alpha(k) + \beta(k) = V_0(k) = Z_{\mathrm{in}}(k)I_0(k) = \frac{Z_{\mathrm{in}}}{Z(k)}\left(\alpha(k) - \beta(k)\right)$$

which implies

$$\beta(k) = \frac{Z_{\mathrm{in}} - Z(k)}{Z_{\mathrm{in}} + Z(k)}\alpha(k) \quad \Rightarrow \quad Z(k)I_0(k) = \alpha(k) - \beta(k) = \frac{2Z(k)}{Z_{\mathrm{in}} + Z(k)}\alpha(k)$$

The antenna impedance has an approximate expression obtained by the induced-emf method. The result is [15, 24]

$$Z_{\text{in}}(k) = -\frac{\mathrm{i}Z(k)}{2\pi \sin^2 k\ell}\Big\{4S(k\ell, kd)\cos^2 k\ell - S(2k\ell, kd)\cos 2k\ell \\ - \sin 2k\ell\,(2C(k\ell, kd) - C(2k\ell, kd))\Big\}$$

where the functions $C(x, y)$ and $S(x, y)$ are

$$\begin{cases} C(x,y) = \ln\dfrac{2x}{y} - \dfrac{1}{2}\mathrm{C}_{\text{in}}(2x) + \dfrac{\mathrm{i}}{2}\mathrm{Si}(2x) \\ S(x,y) = \dfrac{1}{2}\mathrm{Si}(2x) + \dfrac{\mathrm{i}}{2}\mathrm{C}_{\text{in}}(2x) - y \end{cases}$$

and the sine integral $\mathrm{Si}(x)$ and the modified cosine integral $\mathrm{C}_{\text{in}}(x)$ are [1, Sec. 5.2]

$$\mathrm{Si}(x) = \int_0^x \frac{\sin x}{x}\,\mathrm{d}x$$

and

$$\mathrm{C}_{\text{in}}(x) = \int_0^x \frac{1-\cos x}{x}\,\mathrm{d}x$$

respectively. The antenna characteristic vector $\boldsymbol{f}(k, \hat{\boldsymbol{r}})$ then has the form

$$\boldsymbol{f}(k, \hat{\boldsymbol{r}}) = -\frac{\mathrm{i}}{\pi}\frac{Z(k)}{Z_{\text{in}}(k) + Z(k)}\frac{\cos(k\ell\cos\vartheta) - \cos(k\ell)}{\sin\vartheta}\hat{\boldsymbol{\vartheta}} \tag{2.5}$$

In fact,

$$\boldsymbol{f}(k, \hat{\boldsymbol{r}})\alpha(k) = \boldsymbol{F}^{\text{A}}(k, \hat{\boldsymbol{r}}) = -\frac{\mathrm{i}Z(k)I_0(k)}{2\pi}\frac{\cos(k\ell\cos\vartheta) - \cos(k\ell)}{\sin\vartheta}\hat{\boldsymbol{\vartheta}} \\ = -\frac{\mathrm{i}}{2\pi}\frac{2Z(k)}{Z_{\text{in}} + Z(k)}\alpha(k)\frac{\cos(k\ell\cos\vartheta) - \cos(k\ell)}{\sin\vartheta}\hat{\boldsymbol{\vartheta}}$$

From (2.5) we see that the cylindrical dipole antenna has its own resonance behavior. Its variation with $k\ell$ is illustrated in Figure 2. The radius of the antenna in this example is $d = 0.01\ell$. The far field pattern is evaluated at its maximum value at $\vartheta = \pi/2$ (horizontal plane), which is the direction of the main lobe in the frequency interval we are using in this paper, $k\ell \in [0, 4.5]$ (at higher frequencies the horizontal plane is not the main lobe). The figure shows maximum radiation at $k\ell \approx 1.9, 4.1$ and zero radiation at $k\ell = \pi$. At the latter frequency the antenna is completely mismatched to the transmission line ($|Z_{\text{in}}| \to \infty$).

3 The scattering cycle

Our aim in this section is to develop a mathematical model for the received signals. We assume there are N antennas illuminating the target as shown in Figure 3. The

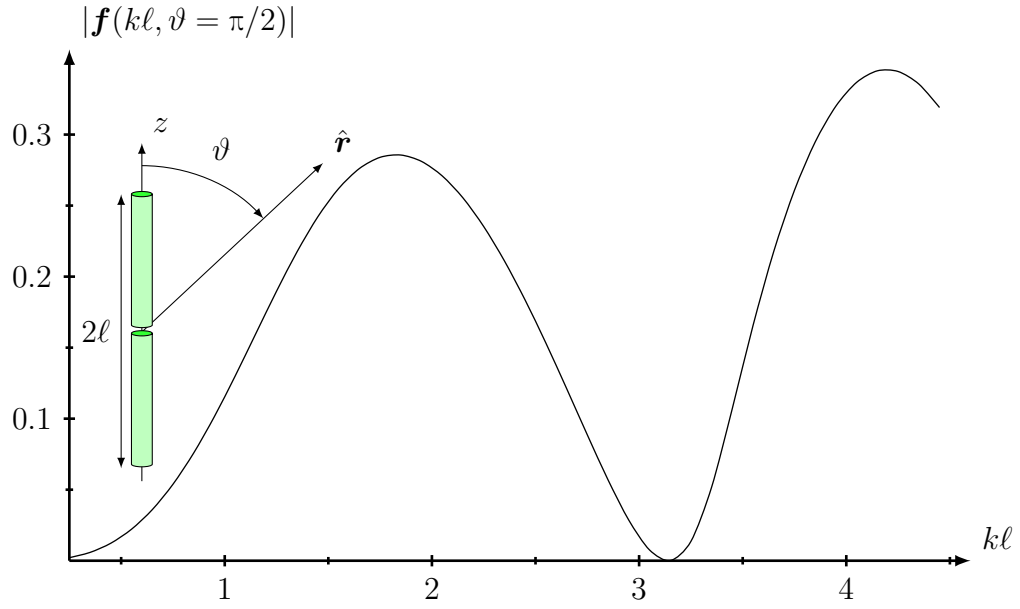

Figure 2: The antenna parameter $|\boldsymbol{f}(k, \vartheta = \pi/2)|$ as a function of $k\ell$ for a cylindrical dipole antenna of length 2ℓ and radius $d = 0.01\ell$.

received signals are the $\beta_i(k)$ in antennas $i = 1, 2, \ldots, N$, due to scattering of the field from an excitation $\alpha_j(k)$ in antenna $j = 1, 2, \ldots, N$. More precisely, we consider the received signal $\beta_i(k)$ after the transmitted signal has been scattered by the obstacle; see Figure 3. Each antenna is characterized in the simplified model (2.2) by the radiation characteristic vector $\boldsymbol{f}_j(k, \hat{\boldsymbol{r}})$, $j = 1, 2, \ldots, N$, which also contains the orientation of the specific antenna. The reference point of each antenna j is given by the local origin O_j, $j = 1, 2, \ldots, N$. We treat each antenna separately, and we neglect coupling between the antennas (in practice, they are separated by a large distance). If several antennas transmit simultaneously, the signal generated by each antenna has to be added by superposition.

The scattered field $\boldsymbol{E}_{\mathrm{s}}(k, \boldsymbol{r})$ by the obstacle in the far zone from excitation $\boldsymbol{E}_0(k, \boldsymbol{r}_0)$ is expressed in the far field amplitude $\boldsymbol{F}_{\mathrm{s}}(k, \hat{\boldsymbol{r}})$ and the scattering dyadic $\mathbf{S}(k, \hat{\boldsymbol{r}}, \hat{\boldsymbol{k}}_{\mathrm{i}})$ as [29]

$$\boldsymbol{E}_{\mathrm{s}}(k, \boldsymbol{r}) \approx \boldsymbol{F}_{\mathrm{s}}(k, \hat{\boldsymbol{r}}) \frac{\mathrm{e}^{\mathrm{i}kr}}{r} = \mathbf{S}(k, \hat{\boldsymbol{r}}, \hat{\boldsymbol{k}}_{\mathrm{i}}) \cdot \boldsymbol{E}_0(k, \boldsymbol{r}_0) \frac{\mathrm{e}^{\mathrm{i}kr}}{r} \tag{3.1}$$

where r is the distance from the local origin O' to the field point. Here $\hat{\boldsymbol{k}}_{\mathrm{i}}$ denotes the direction of energy propagation for $\boldsymbol{E}_0$, *i.e.*, of its Poynting vector. The scatterer can be composed of several different obstacles. Therefore, it suffices to have only one scattering dyadic. If there are several, non-interacting obstacles, the results are added by superposition. Our goal in scattering experiments is to obtain as much information as possible about $\mathbf{S}$.

The scattering dyadic $\mathbf{S}(k, \hat{\boldsymbol{r}}, \hat{\boldsymbol{k}}_{\mathrm{i}})$ is completely characterized by the scattering

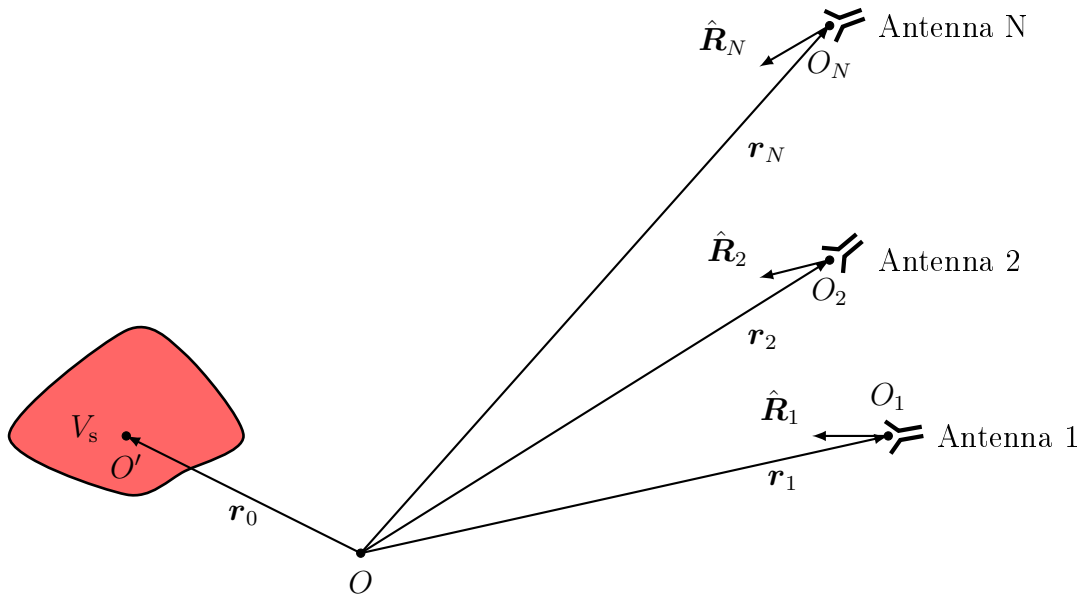

Figure 3: The geometry of the scatterer V_s and its local origin O' and the antennas and their local origins O_i, $i = 1, 2, \ldots, N$. The common origin of the configuration is denoted O. The unit vectors $\hat{\boldsymbol{R}}_i$ are given by $\hat{\boldsymbol{R}}_i = (\boldsymbol{r}_0 - \boldsymbol{r}_i)/|\boldsymbol{r}_0 - \boldsymbol{r}_i|$, $i = 1, 2, \ldots, N$.

transition matrix of the scatterer $T_{nn'}$, and the relation is [29]

$$\mathbf{S}(k, \hat{\boldsymbol{r}}, \hat{\boldsymbol{k}}_\mathrm{i}) = \frac{4\pi}{\mathrm{i}k} \sum_{n,n'} \mathrm{i}^{l'-l+\tau-\tau'} \boldsymbol{A}_n(\hat{\boldsymbol{r}}) T_{nn'}(k) \boldsymbol{A}_{n'}(\hat{\boldsymbol{k}}_\mathrm{i}) \tag{3.2}$$

Here the $\boldsymbol{A}_n$ denote the vector spherical harmonics (see Appendix A).

We find the received signal $\beta_i(k)$ from an excitation in antenna j by analyzing the scattering and receiving process in a series of steps.

1. Assume the amplitude of the transmitting signal on the transmission line in antenna $j = 1, 2, \ldots, N$ is $\alpha_j(k)$.

2. This transmitted signal generates an electric field outside the antenna that radiates energy away from the antenna. Its far field amplitude (2.2) in a general direction $\hat{\boldsymbol{r}}$ is

   $$\boldsymbol{F}_j^\mathrm{A}(k, \hat{\boldsymbol{r}}) = \boldsymbol{f}_j(k, \hat{\boldsymbol{r}}) \alpha_j(k)$$

   The total electric field (2.1) at the local origin of the scatterer O' from antenna j is, in the far-field approximation,

   $$\boldsymbol{E}_j(k, \boldsymbol{r}_0) \approx \boldsymbol{F}_j^\mathrm{A}(k, \hat{\boldsymbol{R}}_j) \frac{\mathrm{e}^{\mathrm{i}kR_j}}{R_j} = \boldsymbol{f}_j(k, \hat{\boldsymbol{R}}_j) \alpha_j(k) \frac{\mathrm{e}^{\mathrm{i}kR_j}}{R_j}$$

   where the distance between antenna j and the scatterer is $R_j = |\boldsymbol{r}_0 - \boldsymbol{r}_j|$ in the direction $\hat{\boldsymbol{R}}_j = (\boldsymbol{r}_0 - \boldsymbol{r}_j)/R_j$ (unit vector in the direction $\boldsymbol{r}_0 - \boldsymbol{r}_j$).

3. The scattered field (3.1) at the local origin $\boldsymbol{r}_i$ of antenna i is

$$\boldsymbol{E}_{\mathrm{s}}(k,\boldsymbol{r}_i) \approx \boldsymbol{F}_{\mathrm{s}}(k,-\hat{\boldsymbol{R}}_i)\frac{\mathrm{e}^{\mathrm{i}kR_i}}{R_i} = \mathbf{S}(k,-\hat{\boldsymbol{R}}_i,\hat{\boldsymbol{R}}_j)\cdot\boldsymbol{E}_j(k,\boldsymbol{r}_0)\frac{\mathrm{e}^{\mathrm{i}kR_i}}{R_i}$$

where $\boldsymbol{F}_{\mathrm{s}}(k,\hat{\boldsymbol{r}})$ is the far field amplitude and $\mathbf{S}(k,\hat{\boldsymbol{r}},\hat{\boldsymbol{k}}_{\mathrm{i}})$ is the scattering dyadic of the scatterer, respectively.

4. The received signal (2.4) in antenna i is

$$\beta_i(k) = \frac{2\pi\mathrm{i}}{k}\boldsymbol{f}_i(k,\hat{\boldsymbol{R}}_i)\cdot\boldsymbol{E}_{\mathrm{s}}(k,\boldsymbol{r}_i) = \frac{2\pi\mathrm{i}}{k}\boldsymbol{f}_i(k,\hat{\boldsymbol{R}}_i)\cdot\mathbf{S}(k,-\hat{\boldsymbol{R}}_i,\hat{\boldsymbol{R}}_j)\cdot\boldsymbol{E}_j(k,\boldsymbol{r}_0)\frac{\mathrm{e}^{\mathrm{i}kR_i}}{R_i}$$

where we have taken $\hat{\boldsymbol{k}}_{\mathrm{i}} = -\hat{\boldsymbol{R}}_i$.

5. We collect the results:

$$\beta_i(k) = \frac{2\pi\mathrm{i}}{kR_iR_j}\mathrm{e}^{\mathrm{i}k(R_i+R_j)}\boldsymbol{f}_i(k,\hat{\boldsymbol{R}}_i)\cdot\mathbf{S}(k,-\hat{\boldsymbol{R}}_i,\hat{\boldsymbol{R}}_j)\cdot\boldsymbol{f}_j(k,\hat{\boldsymbol{R}}_j)\alpha_j(k).$$

This is the received signal in antenna i, due to an excitation in antenna j, and the dimensionless amplification factor $\tilde{\Lambda}_{ij}$ becomes

$$\tilde{\Lambda}_{ij}(k) = \frac{\beta_i(k)}{\alpha_j(k)} = \frac{2\pi\mathrm{i}k}{kR_ikR_j}\mathrm{e}^{\mathrm{i}k(R_i+R_j)}\boldsymbol{f}_i(k,\hat{\boldsymbol{R}}_i)\cdot\mathbf{S}(k,-\hat{\boldsymbol{R}}_i,\hat{\boldsymbol{R}}_j)\cdot\boldsymbol{f}_j(k,\hat{\boldsymbol{R}}_j). \quad (3.3)$$

Here the transmitting and receiving antennas are approximately modeled by $\boldsymbol{f}_j(k,\hat{\boldsymbol{r}})$ and $\boldsymbol{f}_i(k,\hat{\boldsymbol{r}})$, respectively, and the scatterer is modeled by the scattering dyadic $\mathbf{S}(k,\hat{\boldsymbol{r}},\hat{\boldsymbol{k}}_{\mathrm{i}})$. The diagonal terms in the $N\times N$ matrix $\tilde{\boldsymbol{\Lambda}}(k)$ correspond to the signal received by the same antenna and the off-diagonal entries denote the received signal by the other antennas. The vector of transmitted signals $\boldsymbol{\alpha}$ is mapped by $\tilde{\boldsymbol{\Lambda}}$ as

$$\sum_j \tilde{\Lambda}_{ij}\alpha_j = \sum_j \frac{\beta_i}{\alpha_j}\alpha_j = N\beta_i$$

Consequently we define $\boldsymbol{\Lambda} = \frac{1}{N}\tilde{\boldsymbol{\Lambda}}$ as an $N\times N$ matrix that satisfies $\boldsymbol{\beta} = \boldsymbol{\Lambda}\boldsymbol{\alpha}$.

In matrix notation the map from transmitted signals $\boldsymbol{\alpha}(k)$ to the corresponding received signals $\boldsymbol{\beta}(k)$ is thus

$$\boldsymbol{\beta}(k) = \boldsymbol{\Lambda}(k)\boldsymbol{\alpha}(k) = \mathbf{D}(k)\boldsymbol{\Delta}(k)\mathbf{D}(k)\boldsymbol{\alpha}(k), \quad (3.4)$$

where $\mathbf{D}(k)$ is the $N\times N$ diagonal matrix with entries $\mathrm{e}^{\mathrm{i}kR_i}/(kR_i)$, *i.e.*,

$$D_{ij} = \delta_{i,j}\frac{\mathrm{e}^{\mathrm{i}kR_i}}{kR_i}$$

and

$$\Delta_{ij}(k) = \frac{2\pi\mathrm{i}}{N}k\boldsymbol{f}_i(k,\hat{\boldsymbol{R}}_i)\cdot\mathbf{S}(k,-\hat{\boldsymbol{R}}_i,\hat{\boldsymbol{R}}_j)\cdot\boldsymbol{f}_j(k,\hat{\boldsymbol{R}}_j). \quad (3.5)$$

Both $\boldsymbol{\Delta}$ and $\boldsymbol{\Lambda}$ are dimensionless. Under the assumption that the scatterer consists of a reciprocal material (*e.g.*, a dielectric material), the matrices $\boldsymbol{\Delta}$ and $\boldsymbol{\Lambda}$ are symmetric matrices, since [29]

$$\mathbf{S}(k, \hat{\boldsymbol{r}}, \hat{\boldsymbol{k}}_{\mathrm{i}}) = \mathbf{S}^{\mathrm{T}}(k, -\hat{\boldsymbol{k}}_{\mathrm{i}}, -\hat{\boldsymbol{r}}).$$

where the superscript T denotes transpose. The matrices $\boldsymbol{\Delta}(k)\boldsymbol{\Delta}^*(k)$, $\boldsymbol{\Delta}^*(k)\boldsymbol{\Delta}(k)$, $\boldsymbol{\Lambda}(k)\boldsymbol{\Lambda}^*(k)$, and $\boldsymbol{\Lambda}^*(k)\boldsymbol{\Lambda}(k)$ are Hermitian, and, consequently, their eigenvalues are real and the eigenvectors corresponding to different eigenvalues are orthogonal. We note that because of the symmetry, the operation of taking the complex conjugate of $\boldsymbol{\Lambda}$ is the same as taking the adjoint.

3.1 Resonance Enhancement

The idea of the Resonance Enhancement Method is to amplify the peaks of $\mathbf{S}$ by experimentally producing multiples of $\mathbf{S}(k)$ and its adjoint. These peaks correspond to resonances, which in theory are independent of the directions of the incident and scattered fields. The challenge, however, is that $\mathbf{S}$ cannot be directly measured; rather, what is measured is $\boldsymbol{\Lambda}(k)$. On the other hand, many of the factors in (3.3) are known and can be removed. In particular, we assume that the antenna system response factors $\boldsymbol{f}_j$ are all known. The process of removing the system response is called *equalization*.

We note that the vectors $\boldsymbol{f}_i$ in (3.3) depend not only on the frequency k, but also on the direction $\hat{\boldsymbol{R}}_i$ from antenna to target. We assume that this direction is known from beamforming or antenna steering.

For the process of removing known factors, it is more convenient to write (3.4) and (3.5) in an expanded matrix notation. We construct a long vector in which the first 3 elements correspond to the 3 polarization components of the first antenna, the next 3 elements correspond to the 3 polarization components of the second antenna, etc. In particular, we denote by $\mathbf{F}$ the $3N \times N$ matrix

$$\begin{aligned}
\mathbf{F} &= \begin{pmatrix} \boldsymbol{f}_1 & 0 & 0 & \cdots & 0 \\ 0 & \boldsymbol{f}_2 & 0 & \cdots & 0 \\ 0 & 0 & \boldsymbol{f}_3 & \cdots & 0 \\ \vdots & \vdots & \vdots & \cdots & 0 \\ 0 & 0 & 0 & \cdots & \boldsymbol{f}_N \end{pmatrix} = \begin{pmatrix} f_{1,1} & 0 & 0 & \cdots & 0 \\ f_{1,2} & 0 & 0 & \cdots & 0 \\ f_{1,3} & 0 & 0 & \cdots & 0 \\ 0 & f_{2,1} & 0 & \cdots & 0 \\ \vdots & \vdots & \vdots & \cdots & \vdots \\ 0 & 0 & 0 & \cdots & f_{N,3} \end{pmatrix} \\
&= \underbrace{\begin{pmatrix} \widehat{\boldsymbol{f}}_1 & 0 & 0 & \cdots & 0 \\ 0 & \widehat{\boldsymbol{f}}_2 & 0 & \cdots & 0 \\ 0 & 0 & \widehat{\boldsymbol{f}}_3 & \cdots & 0 \\ \vdots & \vdots & \vdots & \cdots & 0 \\ 0 & 0 & 0 & \cdots & \widehat{\boldsymbol{f}}_N \end{pmatrix}}_{\widetilde{\mathbf{F}}} \underbrace{\begin{pmatrix} |\boldsymbol{f}_1| & 0 & 0 & \cdots & 0 \\ 0 & |\boldsymbol{f}_2| & 0 & \cdots & 0 \\ 0 & 0 & |\boldsymbol{f}_3| & \cdots & 0 \\ \vdots & \vdots & \vdots & \cdots & 0 \\ 0 & 0 & 0 & \cdots & |\boldsymbol{f}_N| \end{pmatrix}}_{\mathbf{M}}
\end{aligned}$$

where the $\boldsymbol{f}_j = (f_{j,1}, f_{j,2}, f_{j,3})^T$ are 3×1 column vectors and where the hats denote (possibly complex) unit vectors: $\widehat{\boldsymbol{f}}_j = \boldsymbol{f}_j/|\boldsymbol{f}_j|$. Here $\mathbf{M}$ is a nonsingular $N \times N$ matrix, and $\widehat{\boldsymbol{f}}_i$ corresponds to the polarization of the field at the target due to illumination from antenna i.

The $\mathbf{S}$ matrix also expands to accommodate each polarization and each antenna separately. We denote the expanded $3N \times 3N$ scattering matrix by $\tilde{\mathbf{S}}$, and the diagonal matrix whose elements consist of the expanded vector of antenna beam patterns by $\tilde{\mathbf{F}}$. We can then write (3.4) as $\boldsymbol{\beta} = \boldsymbol{\Lambda}\boldsymbol{\alpha}$ where

$$\boldsymbol{\Lambda} = \mathbf{D}\mathbf{M}\tilde{\mathbf{F}}^{\mathrm{T}}\tilde{\mathbf{S}}\tilde{\mathbf{F}}\mathbf{M}\mathbf{D} = \mathbf{M}[\mathbf{D}\tilde{\mathbf{F}}^{\mathrm{T}}\tilde{\mathbf{S}}\tilde{\mathbf{F}}\mathbf{D}]\mathbf{M}. \tag{3.6}$$

We note that $\mathbf{D}$ and $\mathbf{M}$ commute because they are both diagonal.

We write (3.6) as $\boldsymbol{\Lambda} = \mathbf{Q}\mathcal{S}\mathbf{Q}$, where $\mathbf{Q}$ contain known factors whose effect we can remove, and it is $\mathcal{S}^n$ that we construct iteratively. The factors $\mathbf{Q}$ and $\mathcal{S}$ are defined differently, depending on which quantities are known. In particular, we consider the following cases:

1. None of the system parameters or ranges from antennas to target are known. In this case, we take $\mathbf{Q} = \mathbf{I}$ and $\mathcal{S} = \boldsymbol{\Lambda}$. This corresponds to the case in which no equalization is attempted during the iterative resonance enhancement process.

2. The matrix $\mathbf{F}(k)$ is known, but the ranges from the antennas to the target are unknown. In this case, we take $\mathbf{Q} = \mathbf{M}$, and $\mathcal{S} = \mathbf{D}\tilde{\mathbf{F}}^{\mathrm{T}}\tilde{\mathbf{S}}\tilde{\mathbf{F}}\mathbf{D}$. Here $\mathcal{S}$ is an $N \times N$ matrix.

3. The antenna characteristics matrix $\mathbf{F}$ is unknown, but the ranges of $\mathbf{D}$ are known. In this case we take $\mathbf{Q} = \mathbf{D}$ and $\mathcal{S} = \mathbf{M}\tilde{\mathbf{F}}^{T}\tilde{\mathbf{S}}\tilde{\mathbf{F}}\mathbf{M}$.

4. Not only is the matrix $\mathbf{F}$ known, but the ranges from the antennas to the target are also known, and hence the matrix $\mathbf{D}$ is known. In this case, we take $\mathbf{Q} = \mathbf{M}\mathbf{D}$ and $\mathcal{S}(k) = \tilde{\mathbf{F}}^{\mathrm{T}}\tilde{\mathbf{S}}\tilde{\mathbf{F}}$. The matrix $\mathbf{Q}$ includes both the system responses and propagation factors.

In the REM process, we begin with a vector of initial signals $\boldsymbol{\alpha}^0(k)$ on the antenna array. The signals $\boldsymbol{\alpha}^0(k)$ give rise to transmitted fields which scatter from the target and give rise to the associated vector of received signals $\boldsymbol{\beta}^0(k) = \boldsymbol{\Lambda}(k)\boldsymbol{\alpha}^0(k)$. The received signals $\boldsymbol{\beta}^0(k)$ are then corrected for the antenna responses and possibly also for propagation, by multiplying by the weight matrix $\mathbf{Q}^{-1}(k)$. The resulting signals are complex conjugated, which in the time domain corresponds to time-reversing them. The result is a candidate for a new signal to be transmitted. We amplify all these signals by the same scalar normalizing factor of A, which is chosen so that each successive transmitted vector $\boldsymbol{\alpha}$ of waveforms has the same total energy $\pi^{-1}\sum_j \int |\alpha_j^0(k)|^2/Z(k)\ \mathrm{d}k$ (see appendix), and before transmitting, we again multiply the resulting signals by $\mathbf{Q}^{-1}(k)$ to pre-distort them to correct for the transmitting antennas and possibly also the propagation path. Thus the next signal in

the REM iteration process is

$$\begin{aligned}\boldsymbol{\alpha}^1(k) &= \mathbf{Q}^{-1}(k)A\left(\mathbf{Q}^{-1}(k)\boldsymbol{\beta}^0(k)\right)^* = \mathbf{Q}^{-1}(k)A\left(\mathbf{Q}^{-1}(k)\boldsymbol{\Lambda}(k)\boldsymbol{\alpha}^0(k)\right)^* \\ &= \mathbf{Q}^{-1}(k)A\mathbf{Q}^{-1}(k)\mathbf{Q}(k)\mathcal{S}^*(k)\mathbf{Q}(k)\left(\boldsymbol{\alpha}^0(k)\right)^* \\ &= \mathbf{Q}^{-1}(k)A\mathcal{S}^*(k)\mathbf{Q}(k)\left(\boldsymbol{\alpha}^0(k)\right)^*.\end{aligned}$$

Here $*$ denotes complex conjugation. At the next step, the new signal to be transmitted is

$$\begin{aligned}\boldsymbol{\alpha}^2(k) &= \mathbf{Q}^{-1}(k)A\left(\mathbf{Q}^{-1}(k)\boldsymbol{\beta}^1(k)\right)^* = \mathbf{Q}^{-1}(k)A\mathbf{Q}^{-1}(k)\left[\boldsymbol{\Lambda}(k)\boldsymbol{\alpha}^1(k)\right]^* \\ &= \mathbf{Q}^{-1}(k)A\mathbf{Q}^{-1}(k)[\mathbf{Q}(k)\mathcal{S}(k)\mathbf{Q}(k)]^*\left[\mathbf{Q}^{-1}(k)A\mathcal{S}^*(k)\mathbf{Q}(k)\left(\boldsymbol{\alpha}^0(k)\right)^*\right]^* \\ &= \mathbf{Q}^{-1}(k)A\mathcal{S}^*(k)A^*\mathcal{S}(k)\mathbf{Q}(k)\boldsymbol{\alpha}^0(k) \\ &= \mathbf{R}(k)\boldsymbol{\alpha}^0(k),\end{aligned}$$

where the time reversal matrix is

$$\mathbf{R}(k) = \mathbf{Q}^{-1}(k)|A|^2\mathcal{S}^*(k)\mathcal{S}(k)\mathbf{Q}(k). \tag{3.7}$$

Because $\mathcal{S}$ is symmetric, the matrices $\mathcal{S}^*(k)\mathcal{S}(k)$ and $\mathbf{R}$ are Hermitian, and consequently their eigenvalues are real and the eigenvectors corresponding to different eigenvalues are orthogonal.

We see that after even or odd numbers of iterations, the transmitted signals are

$$\boldsymbol{\alpha}^{2n}(k) = \mathbf{R}^n(k)\boldsymbol{\alpha}^0(k), \quad \boldsymbol{\alpha}^{2n-1}(k) = A\mathbf{Q}^{-1}(k)\mathcal{S}^*(k)\mathbf{Q}(k)\mathbf{R}^{n-1}(k)(\boldsymbol{\alpha}^0(k))^*,$$

where

$$\mathbf{R}^n(k) = |A|^{2n}\mathbf{Q}^{-1}(k)\left[\mathcal{S}^*(k)\mathcal{S}(k)\right]^n\mathbf{Q}(k).$$

We note that the effect of $2n$ iterations of the REM process is to raise the product $\mathcal{S}^*(k)\mathcal{S}(k)$ to the nth power. Although we do not explicitly treat noise in this paper, we note that noise is different at each iteration and consequently the REM process improves the signal-to-noise ratio for $[\mathcal{S}^*(k)\mathcal{S}(k)]^n$.

The question of what time-domain waveforms the process converges to can be answered by noting that as the iterations proceed, peaks in the frequency domain sharpen. Thus the REM iterations in general converge to a single frequency waveform whose frequency is that at which the largest eigenvalue of $\mathbf{R}$ is greatest. [10, 22, 26].

The application of $\mathbf{Q}^{-1}$ can involve some practical difficulties. In particular, $\mathbf{Q}^{-1}$ corresponds to an infinite impulse response (IIR) filter, whose application in the time domain can involve an infinite-duration signal. Various techniques are known [23] for approximating an IIR filter by a finite impulse response (FIR) filter and these could be used here.

4 Simple examples

4.1 One single cylindrical dipole antenna

Let the antenna be a cylindrical dipole antenna of length 2ℓ and radius d, (see Section 2.1) located at $\boldsymbol{R}_1 = -R_1\hat{\boldsymbol{z}}$, as shown in Figure 4. From (2.5), the far field

Figure 4: The geometry of the spherical scatterer (radius a) and the linear antenna at $\boldsymbol{R}_1 = -R_1\hat{\boldsymbol{z}}$ and $\vartheta = \pi/2$. The antenna is in the far field of the spherical scatterer.

pattern of the antenna is

$$\boldsymbol{f}(k,\hat{\boldsymbol{r}}) = -\frac{\mathrm{i}}{\pi}\frac{Z}{Z_{\mathrm{in}}+Z}\frac{\cos\left(k\ell\cos\vartheta\right)-\cos(k\ell)}{\sin\vartheta}\hat{\boldsymbol{\vartheta}}.$$

The scattering cycle in Section 3 results in ($\hat{\boldsymbol{R}}_1 = -\hat{\boldsymbol{z}}$) [see (3.3)]

$$\Lambda_{11}(k) = 2\pi\mathrm{i}k\frac{\mathrm{e}^{2\mathrm{i}kR_1}}{k^2R_1^2}\boldsymbol{f}(k,-\hat{\boldsymbol{z}})\cdot\mathbf{S}(k,\hat{\boldsymbol{z}},-\hat{\boldsymbol{z}})\cdot\boldsymbol{f}(k,-\hat{\boldsymbol{z}})$$

Let the scatterer be a homogeneous, dielectric, spherical scatterer of radius a. Then $T_{nn'} = \delta_{\tau\tau'}\delta_{\sigma\sigma'}\delta_{mm'}\delta_{ll'}t_{\tau l}$, and the scattering dyadic in the backscattering direction is [29, p. 389]

$$\mathbf{S}(k,\hat{\boldsymbol{z}},-\hat{\boldsymbol{z}}) = -\frac{1}{2\mathrm{i}k}\mathbf{I}_2 s_{\mathrm{b}}(k)$$

where $\mathbf{I}_2$ is the two-dimensional unit dyadic, and where

$$s_{\mathrm{b}}(k) = \sum_{l=1}^{\infty}(2l+1)(-1)^l\left(t_{1l}(k)-t_{2l}(k)\right) \tag{4.1}$$

The transition matrix entries are

$$t_{\tau l} = -\frac{\mathrm{j}_l(ka)(k_1a\mathrm{j}_l(k_1a))' - \gamma_\tau(ka\mathrm{j}_l(ka))'\mathrm{j}_l(k_1a)}{\mathrm{h}_l^{(1)}(ka)(k_1a\mathrm{j}_l(k_1a))' - \gamma_\tau(ka\mathrm{h}_l^{(1)}(ka))'\mathrm{j}_l(k_1a)},$$

where ϵ_1 and μ_1 are the permittivity and the permeability of the material inside the sphere, and

$$\gamma_\tau = \delta_{\tau 1}\frac{\mu_1}{\mu} + \delta_{\tau 2}\frac{\epsilon_1}{\epsilon}.$$

The lambda factor then becomes (note that $-\hat{\boldsymbol{z}}$ corresponds to $\vartheta = \pi/2$)

$$\Lambda_{11}(k) = \frac{\mathrm{e}^{2\mathrm{i}kR_1}}{k^2R_1^2\pi}s_{\mathrm{b}}(k)\left(\frac{Z}{Z_{\mathrm{in}}+Z}\left(1-\cos(k\ell)\right)\right)^2, \tag{4.2}$$

and, with equalization Option 4 of Section 3.1, the time reversal matrix is [see (3.7)]

$$R_{\mathrm{eq}}(k) = \left|s_{\mathrm{b}}(k)\right|^2 \quad \text{(equalized)} \tag{4.3}$$

or alternatively, if we assume the range R_1 is known, then with (non-) equalization Option 3 of Section 3.1, we have

$$R(k) = \left| \frac{Z}{Z_{\text{in}} + Z} \left(1 - \cos(k\ell)\right) \right|^4 |s_{\text{b}}(k)|^2 . \quad \text{(not equalized)} \tag{4.4}$$

4.2 Two cylindrical dipole antennas

The two cylindrical dipole antennas, located at $\boldsymbol{r}_1$ and $\boldsymbol{r}_2$, respectively [see Figure 5], generate an amplification factor

$$\begin{aligned} \boldsymbol{\Lambda}(k) &= 2\pi \mathrm{i} k \begin{pmatrix} \frac{\mathrm{e}^{2\mathrm{i}kR_1}}{k^2 R_1^2} a(k) & \frac{\mathrm{e}^{\mathrm{i}k(R_1+R_2)}}{k^2 R_1 R_2} b(k) \\ \frac{\mathrm{e}^{\mathrm{i}k(R_1+R_2)}}{k^2 R_1 R_2} c(k) & \frac{\mathrm{e}^{2\mathrm{i}kR_2}}{k^2 R_2^2} d(k) \end{pmatrix} \\ &= 2\pi \mathrm{i} k \begin{pmatrix} \frac{\mathrm{e}^{\mathrm{i}kR_1}}{kR_1} & 0 \\ 0 & \frac{\mathrm{e}^{\mathrm{i}kR_2}}{kR_2} \end{pmatrix} \begin{pmatrix} a(k) & b(k) \\ c(k) & d(k) \end{pmatrix} \begin{pmatrix} \frac{\mathrm{e}^{\mathrm{i}kR_1}}{kR_1} & 0 \\ 0 & \frac{\mathrm{e}^{\mathrm{i}kR_2}}{kR_2} \end{pmatrix}, \end{aligned}$$

where

$$\begin{cases} a(k) = \boldsymbol{f}_1(k, \hat{\boldsymbol{R}}_1) \cdot \mathbf{S}(k, -\hat{\boldsymbol{R}}_1, \hat{\boldsymbol{R}}_1) \cdot \boldsymbol{f}_1(k, \hat{\boldsymbol{R}}_1) \\ b(k) = c(k) = \boldsymbol{f}_2(k, \hat{\boldsymbol{R}}_2) \cdot \mathbf{S}(k, -\hat{\boldsymbol{R}}_2, \hat{\boldsymbol{R}}_1) \cdot \boldsymbol{f}_1(k, \hat{\boldsymbol{R}}_1) \\ d(k) = \boldsymbol{f}_2(k, \hat{\boldsymbol{R}}_2) \cdot \mathbf{S}(k, -\hat{\boldsymbol{R}}_2, \hat{\boldsymbol{R}}_2) \cdot \boldsymbol{f}_2(k, \hat{\boldsymbol{R}}_2). \end{cases}$$

Here we specify the positions of the antennas as $\boldsymbol{R}_1 = -R_1 \hat{\boldsymbol{z}}$ and $\boldsymbol{R}_2 = R_2 \hat{\boldsymbol{R}}_2$, where $\hat{\boldsymbol{R}}_2 = -\hat{\boldsymbol{x}} \sin\theta - \hat{\boldsymbol{z}} \cos\theta$. Note that with our definition of the angle θ in Figure 5, the scattering angle[2] is not θ but $\pi - \theta$. Note also that we have arranged the two cylindrical dipole antennas in the same direction. Other configurations are, of course, possible.

For the homogeneous, dielectric, spherical scatterer in Section 4.1, we have [29, p. 387]

$$\begin{pmatrix} S_{\parallel\parallel}(k, \hat{\boldsymbol{r}}, \hat{\boldsymbol{z}}) & S_{\parallel\perp}(k, \hat{\boldsymbol{r}}, \hat{\boldsymbol{z}}) \\ S_{\perp\parallel}(k, \hat{\boldsymbol{r}}, \hat{\boldsymbol{z}}) & S_{\perp\perp}(k, \hat{\boldsymbol{r}}, \hat{\boldsymbol{z}}) \end{pmatrix} = \frac{1}{\mathrm{i}k} \begin{pmatrix} S_1(k) & 0 \\ 0 & S_4(k) \end{pmatrix},$$

where the two diagonal elements $S_1(k)$ and $S_4(k)$ are defined as

$$\begin{cases} S_1(k) = \sum_{l=1}^{\infty} \frac{2l+1}{l(l+1)} \left(\pi_l(-\cos\theta) t_{1l} + \tau_l(-\cos\theta) t_{2l}\right) \\ S_4(k) = \sum_{l=1}^{\infty} \frac{2l+1}{l(l+1)} \left(\pi_l(-\cos\theta) t_{2l} + \tau_l(-\cos\theta) t_{1l}\right) \end{cases},$$

where ($\mathrm{P}_l(x)$ denotes the Legendre polynomials)

$$\begin{cases} \pi_l(x) = \mathrm{P}_l'(x) \\ \tau_l(x) = l(l+1)\mathrm{P}_l(x) - x\mathrm{P}_l'(x) \end{cases}.$$

[2] The cosine of the scattering angle is defined as the scalar product between the incident direction and the observed one.

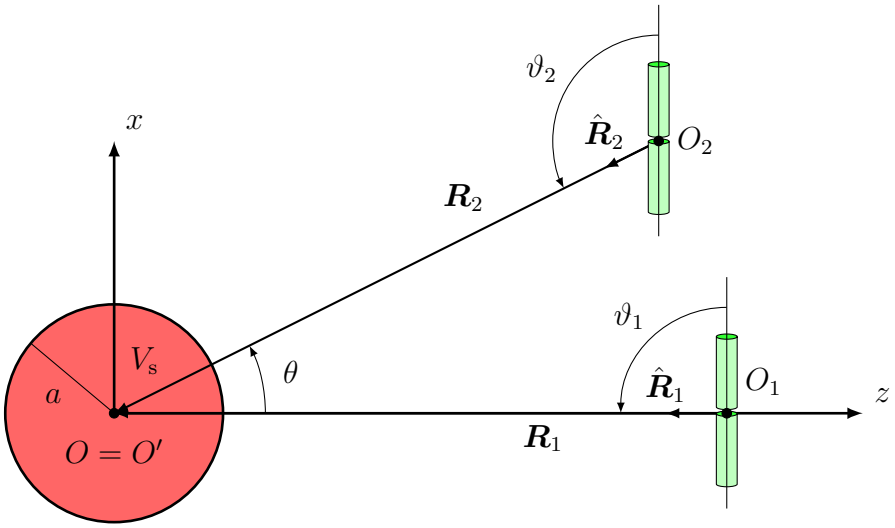

Figure 5: The geometry of the spherical scatterer (radius a) and two simple horizontal electrical dipoles at $\boldsymbol{R}_1 = -R_1\hat{\boldsymbol{z}}$ and $\boldsymbol{R}_2 = -R_2\,(\hat{\boldsymbol{x}}\sin\theta + \hat{\boldsymbol{z}}\cos\theta)$. The antennas are in the far field of the spherical scatterer.

In spherical unit vectors, the scattering dyadic becomes [29, p. 206] (In the geometry of Figure 5, we have $\hat{\boldsymbol{e}}_{\mathrm{i}\parallel} = \hat{\boldsymbol{x}}$, $\hat{\boldsymbol{e}}_{\mathrm{s}\parallel} = -\hat{\boldsymbol{\theta}} = -\hat{\boldsymbol{x}}\cos\theta + \hat{\boldsymbol{z}}\sin\theta$, and $\hat{\boldsymbol{e}}_{\mathrm{i}\perp} = \hat{\boldsymbol{e}}_{\mathrm{s}\perp} = -\hat{\boldsymbol{y}}$)

$$\begin{aligned}\mathbf{S}(k, -\hat{\boldsymbol{R}}_2, -\hat{\boldsymbol{z}}) &= -\hat{\boldsymbol{\theta}} S_{\parallel\parallel}(k, -\hat{\boldsymbol{R}}_2, -\hat{\boldsymbol{z}})\hat{\boldsymbol{x}} \;+\; \hat{\boldsymbol{y}} S_{\perp\perp}(k, -\hat{\boldsymbol{R}}_2, -\hat{\boldsymbol{z}})\hat{\boldsymbol{y}} \\ &= -\frac{\hat{\boldsymbol{\theta}} S_1 \hat{\boldsymbol{x}}}{\mathrm{i}k} + \frac{\hat{\boldsymbol{y}} S_4 \hat{\boldsymbol{y}}}{\mathrm{i}k}\end{aligned} \tag{4.5}$$

and for the two back scattering contributions we have

$$\mathbf{S}(k, \hat{\boldsymbol{z}}, -\hat{\boldsymbol{z}}) = -\frac{1}{2\mathrm{i}k}\mathbf{I}_2 s_{\mathrm{b}}(k), \quad \mathbf{S}(k, -\hat{\boldsymbol{R}}_2, \hat{\boldsymbol{R}}_2) = -\frac{1}{2\mathrm{i}k}\mathbf{I}_2 s_{\mathrm{b}}(k)$$

where the sum $s_{\mathrm{b}}(k)$ is defined in (4.1).

Let the antennas both be oriented along the x-axis with a phase difference δ. The radiation characteristic vectors $\boldsymbol{f}_1(k, \hat{\boldsymbol{r}})$ and $\boldsymbol{f}_2(k, \hat{\boldsymbol{r}})$ are

$$\boldsymbol{f}_1(k, -\hat{\boldsymbol{z}}) = \frac{\mathrm{i}}{\pi}\frac{Z}{Z_{\mathrm{in}} + Z}\,(1 - \cos(k\ell))\,\hat{\boldsymbol{x}}$$

since $\vartheta_1 = \pi/2$ and $\hat{\boldsymbol{\vartheta}}_1 = -\hat{\boldsymbol{x}}$, and

$$\boldsymbol{f}_2(k, \hat{\boldsymbol{R}}_2) = \frac{\mathrm{i}}{\pi}\mathrm{e}^{\mathrm{i}\delta}\frac{Z}{Z_{\mathrm{in}} + Z}\frac{\cos\left(k\ell\sin\theta\right) - \cos(k\ell)}{\cos\theta}\hat{\boldsymbol{\theta}}$$

since $\vartheta_2 = \pi/2 + \theta$ and $\hat{\boldsymbol{\vartheta}}_2 = -\hat{\boldsymbol{\theta}}$.

The scattering dyadic then simplifies to

$$\begin{cases} a(k) = \boldsymbol{f}_1(k,-\hat{\boldsymbol{z}})\cdot\mathbf{S}(k,\hat{\boldsymbol{z}},-\hat{\boldsymbol{z}})\cdot\boldsymbol{f}_1(k,-\hat{\boldsymbol{z}}) \\ \qquad = \dfrac{1}{2\mathrm{i}k\pi^2}\left(\dfrac{Z}{Z_{\mathrm{in}}+Z}\right)^2(1-\cos(k\ell))^2\, s_{\mathrm{b}}(k) \\ b(k) = c(k) = \boldsymbol{f}_2(k,\hat{\boldsymbol{R}}_2)\cdot\mathbf{S}(k,-\hat{\boldsymbol{R}}_2,-\hat{\boldsymbol{z}})\cdot\boldsymbol{f}_1(k,-\hat{\boldsymbol{z}}) \\ \qquad = \dfrac{\mathrm{e}^{\mathrm{i}\delta}}{\mathrm{i}k\pi^2}\left(\dfrac{Z}{Z_{\mathrm{in}}+Z}\right)^2(1-\cos(k\ell))\left(\dfrac{\cos(k\ell\sin\theta)-\cos(k\ell)}{\cos\theta}\right)S_1(k) \\ d(k) = \boldsymbol{f}_2(k,\hat{\boldsymbol{R}}_2)\cdot\mathbf{S}(k,-\hat{\boldsymbol{R}}_2,\hat{\boldsymbol{R}}_2)\cdot\boldsymbol{f}_2(k,\hat{\boldsymbol{R}}_2) \\ \qquad = \dfrac{\mathrm{e}^{2\mathrm{i}\delta}}{2\mathrm{i}k\pi^2}\left(\dfrac{Z}{Z_{\mathrm{in}}+Z}\right)^2\left(\dfrac{\cos(k\ell\sin\theta)-\cos(k\ell)}{\cos\theta}\right)^2 s_{\mathrm{b}}(k) \end{cases}$$

The time reversal matrix $\mathbf{R}(k)$ in (3.7) can now be formed. Without equalization, *i.e.,* using equalization Option 3 of Section 3.1 with known ranges R_1 and R_2 (and thus removal of $\mathbf{D}$ in (3.4)), we get

$$\mathbf{R}(k) = 4\pi^2k^2\begin{pmatrix} a^*(k) & b^*(k) \\ c^*(k) & d^*(k)\end{pmatrix}\begin{pmatrix} a(k) & b(k) \\ c(k) & d(k)\end{pmatrix} \tag{4.6}$$

We can also form an equalized version of the time reversal matrix (Option 4 in Section 3.1). We obtain

$$\mathbf{R}_{\mathrm{eq}}(k) = \frac{1}{\pi^2}\begin{pmatrix} {s_{\mathrm{b}}}^*(k) & 2\mathrm{e}^{-\mathrm{i}\delta}S_1^*(k) \\ 2\mathrm{e}^{-\mathrm{i}\delta}S_1^*(k) & \mathrm{e}^{-2\mathrm{i}\delta}{s_{\mathrm{b}}}^*(k)\end{pmatrix}\begin{pmatrix} s_{\mathrm{b}}(k) & 2\mathrm{e}^{\mathrm{i}\delta}S_1(k) \\ 2\mathrm{e}^{\mathrm{i}\delta}S_1(k) & \mathrm{e}^{2\mathrm{i}\delta}s_{\mathrm{b}}(k)\end{pmatrix} \tag{4.7}$$

5 Numerical illustrations

In Figure 6, we illustrate the differential scattering cross section in the backward direction (RCS), $\frac{\mathrm{d}\sigma}{\mathrm{d}\Omega}(k,-\hat{\boldsymbol{k}}_{\mathrm{i}},\hat{\boldsymbol{k}}_{\mathrm{i}})/\pi a^2$ as a function of ka for a homogeneous, dielectric sphere of radius a. The definition of the differential scattering cross section in the backward direction (RCS) is [29, p. 207]

$$\frac{\mathrm{d}\sigma}{\mathrm{d}\Omega}(k,-\hat{\boldsymbol{k}}_{\mathrm{i}},\hat{\boldsymbol{k}}_{\mathrm{i}}) = 4\pi\frac{\left|\mathbf{S}(k,-\hat{\boldsymbol{k}}_{\mathrm{i}},\hat{\boldsymbol{k}}_{\mathrm{i}})\cdot\boldsymbol{E}_0(k)\right|^2}{|\boldsymbol{E}_0(k)|^2}$$

where $\boldsymbol{E}_0(k)$ is the amplitude of the incident field at the origin of the scatterer. For a spherical dielectric scatterer, this expression simplifies to [29, p. 390]

$$\frac{\frac{\mathrm{d}\sigma}{\mathrm{d}\Omega}(k,-\hat{\boldsymbol{k}}_{\mathrm{i}},\hat{\boldsymbol{k}}_{\mathrm{i}})}{\pi a^2} = \frac{|s_{\mathrm{b}}(k)|^2}{k^2a^2} = \frac{1}{k^2a^2}\left|\sum_{l=1}^{\infty}(2l+1)(-1)^l\left(t_{1l}(k)-t_{2l}(k)\right)\right|^2 \tag{5.1}$$

where we used the sum $s_{\mathrm{b}}(k)$ defined in (4.1). The explicit values of the permittivity and the permeability of the sphere in the figure are $\epsilon_1/\epsilon = 16$, $\mu_1/\mu = 1$, respectively. This value of the permittivity is chosen for clarity and illustrative value of the figures.

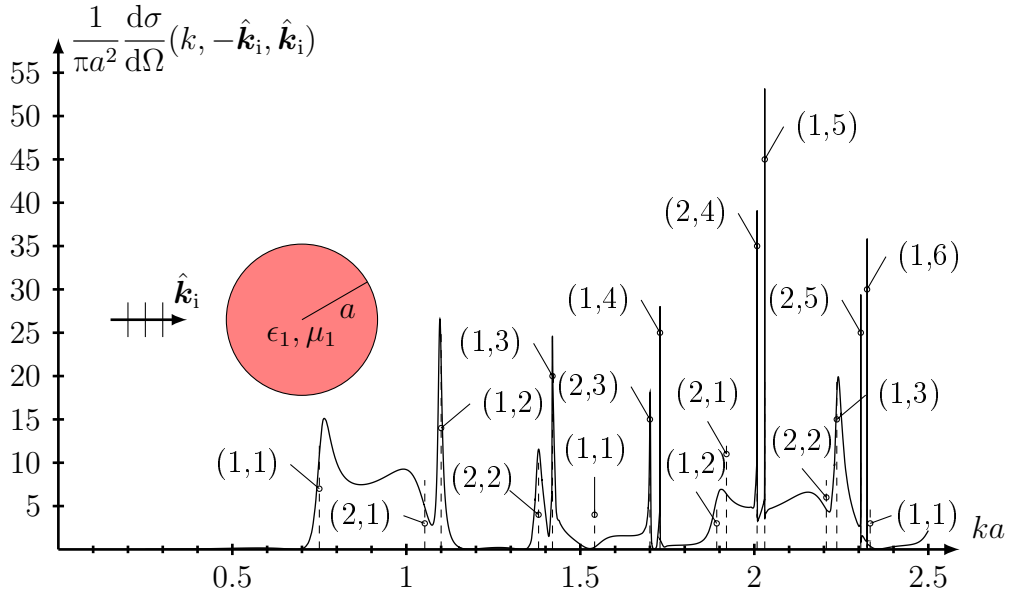

Figure 6: The differential scattering cross section $\frac{\mathrm{d}\sigma}{\mathrm{d}\Omega}(k,-\hat{\boldsymbol{k}}_\mathrm{i},\hat{\boldsymbol{k}}_\mathrm{i})/(\pi a^2)$ in the backward direction as a function of ka for a homogeneous dielectric sphere. The location of the real value of the poles in Table 1 is marked with a dashed curve, and the corresponding (τ, l) values are displayed in parenthesis; see also Figure 7.

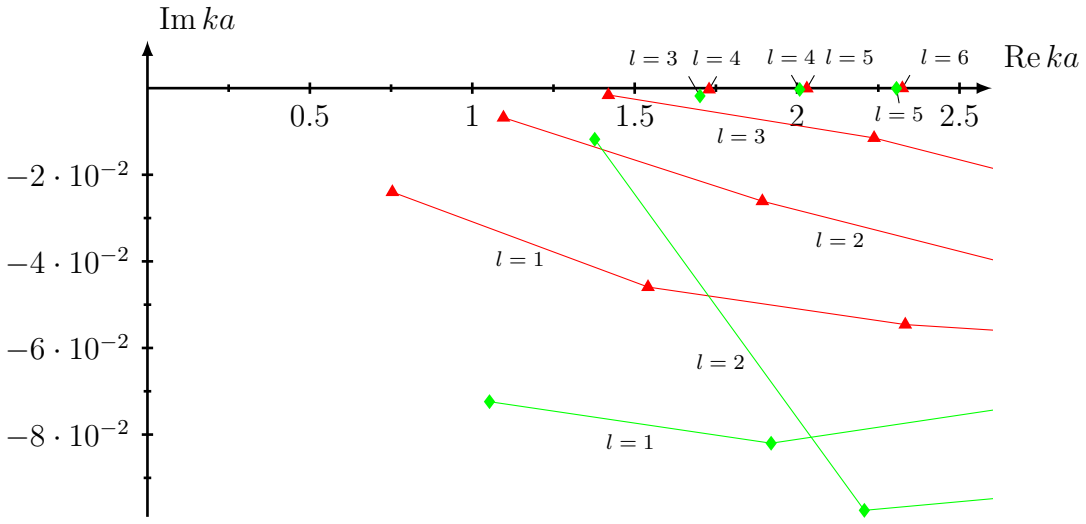

Figure 7: The poles in the complex ka-plane of the transition matrix $t_{\tau l}$. The red triangles mark the poles for $\tau = 1$ and the green diamonds correspond to $\tau = 2$. Note the scale on the imaginary axis.

A smaller value of the permittivity pushes the resonances to higher frequencies with similar resonance structure.

The detailed frequency behavior of the differential scattering cross section in the backward direction depends on the frequency behavior of the transition matrix entries $t_{\tau l}$ in (5.1), which have poles in the lower complex ka plane. These poles give rise to resonances in the differential scattering cross section in the backward direction and in the eigenvalues of $\mathbf{\Lambda}$ or $\mathbf{\Delta}$. Some of these resonances are very sharp and they correspond to poles close to the real ka axis.

The locations of the poles closest to the origin for the geometry in this numerical example are given in Table 1. In Figure 7, we show the locations of the poles in the complex ka plane. Poles with the same l value are connected by lines. From the figure, we observe that the poles appear in families, corresponding to the same τ and l indices. There are no poles in the complex upper-half plane and the poles are symmetrically located in the third and forth quadrant of the complex ka plane (only forth quadrant shown).

The plot of the differential scattering cross section in the backward direction is thus a plot of the behavior on the real axis of a function that is the magnitude squared of a meromorphic complex-valued function. The resonances in Figure 6 correspond uniquely to the poles of the transition matrix, and the location of the first poles with indices (τ, l) are displayed in the figure. Comparing Figures 6 and 7, we notice that the resonances occur approximately at ka corresponding to the real part of the complex pole of a certain transition matrix entry. The closer the pole is to the real axis, the better is the agreement. We also observe that the sharpness of the resonance is related to the value of the imaginary part of the pole — the smaller the imaginary part, the sharper the resonance. The small shift in frequency comes from the "background" part of the meromorphic function that is analytic in the neighborhood of the pole; see [37] and Appendix B. The height of the resonance is related to the residue of the corresponding pole, but it also affected by the properties of the function near the poles. These poles are the singularities of the Singularity Expansion Method (SEM) [3].

5.1 One single antenna

In this first configuration, we employ a single central-fed, cylindrical dipole antenna and a spherical scatterer. The geometry of the antenna in the first pair of examples is specified by $\ell = 1.5a$ and $d/\ell = 0.01$. In Figure 8 and 9, we show the first three powers of the time reversal matrices for the equalized case in (4.3) and for the unequalized case in (4.4) (the matrices are just 1×1 in this case). The equalized case shown in Figure 8 is almost identical to the differential scattering cross section in Figure 6. The only difference is that the curves in Figure 6 are divided by $(ka)^2$ This division diminishes the higher frequencies in Figure 6 and, for this reason, the two figures differ slightly.

When the time reversal matrix is iterated, the largest value of the largest eigenvalue is amplified and all other values diminish. The largest value of the largest eigenvalue corresponds to the position of a largest resonance that is excited in the

τ	l	$z_0 = x_0 - \mathrm{i}y_0$
1	1	$0.754 - 0.0240\mathrm{i}$
2	1	$1.053 - 0.0724\mathrm{i}$
1	2	$1.096 - 0.0068\mathrm{i}$
2	2	$1.377 - 0.0118\mathrm{i}$
1	3	$1.419 - 0.0016\mathrm{i}$
1	1	$1.541 - 0.0459\mathrm{i}$
2	3	$1.701 - 0.0018\mathrm{i}$
1	4	$1.729 - 0.0003\mathrm{i}$

τ	l	$z_0 = x_0 - \mathrm{i}y_0$
1	2	$1.893 - 0.0261\mathrm{i}$
2	1	$1.920 - 0.0820\mathrm{i}$
2	4	$2.008 - 0.0003\mathrm{i}$
1	5	$2.030 - 0.00006\mathrm{i}$
2	2	$2.207 - 0.0975\mathrm{i}$
1	3	$2.237 - 0.0115\mathrm{i}$
2	5	$2.306 - 0.00004\mathrm{i}$
1	6	$2.324 - 0.00001\mathrm{i}$
1	1	$2.333 - 0.0546\mathrm{i}$

Table 1: The locations of the poles z_0 of the transition matrix entries, $t_{\tau l}$, closest to the origin and the real axis in the complex ka-plane for a homogeneous dielectric sphere with material data $\epsilon_1/\epsilon = 16$ and $\mu_1/\mu = 1$.

transition matrix. The position of this pole is shown by a dashed vertical line in the figures. Which resonance that is amplified depends on the excitation. We notice that different resonances are amplified in the equalized and in the unequalized cases. The curves in Figures 8 and 9 illustrate this difference in excitation very clearly. The reason is that in the unequalized case the scattering characteristics, shown by the curve in Figure 8, are multiplied by a frequency taper (antenna characteristics), which is shown by the dashed curve in Figure 9. This frequency taper suppresses certain frequencies — in particular in an interval close to the largest resonance (1,5). This observation emphasizes the importance of equalization.

Figures 8 and 9 also point to a shortcoming of the equalization procedure: if there is no measured signal in a certain frequency band, no amount of equalization can amplify a non-existent signal. Similarly, attempts to amplify a very weak signal in a band are likely to amplify noise in that band.

A slightly smaller antenna, $\ell = 0.9a$ is employed in Figure 10. This figure depicts the behavior of the unequalized data. The equalized behavior is identical to the curves in Figure 8. Since the antenna is smaller, its frequency taper is shifted towards higher frequencies, and, in this case, the amplification occurs close to the largest resonance (1,5).

5.2 Two antennas

In Section 4.2, we analyzed the configuration of two identical cylindrical dipole antennas in a spatially distributed configuration. The time reversal matrices for the unequalized and the equalized cases are given in (4.6) and (4.7), respectively. The largest eigenvalues of $\mathbf{R}$ and $\mathbf{R}_{\mathrm{eq}}$ are illustrated in Figure 11. The antenna parameters in this figure are $\ell = 1.5a$, $d = 0.01\ell$, $\delta = 90^\circ$, and $\theta = 30^\circ$.

The two antennas illuminate the target in a different way (spatially distributed illumination) compared to the one antenna case in Section 4.1, and as a consequence,

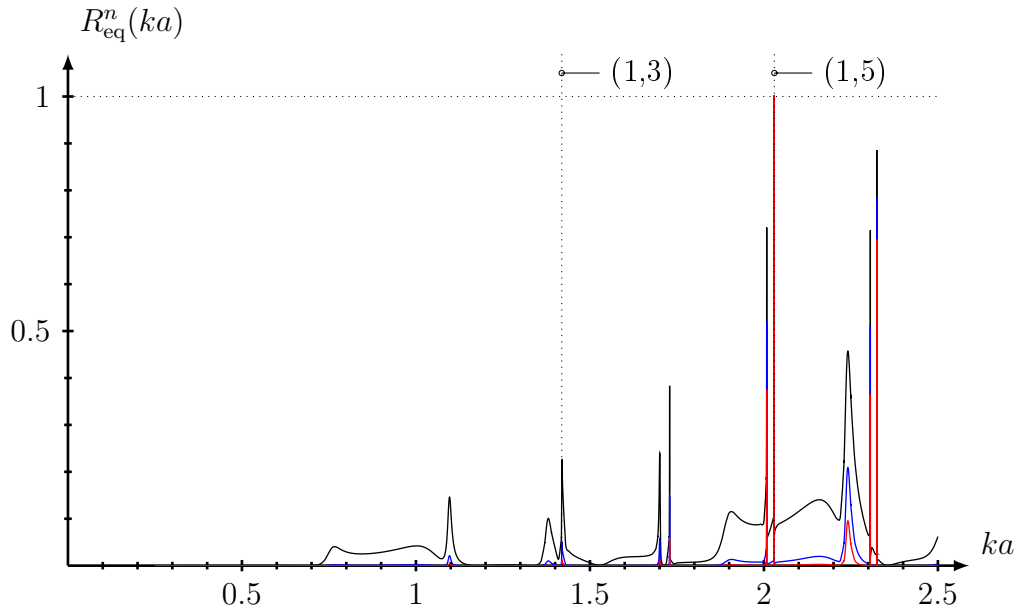

Figure 8: The value of the equalized $R^n_{\rm eq}$ for $n = 1, 2, 3$ for a single cylindrical dipole antenna. The value is normalized with maximum absolute value of $R_{\rm eq}$ in the interval. The position of the first resonance in the transition matrix (1,5) is shown by a dotted vertical line. The second dotted line, (1,3), shows the position of the resonance of the unequalized data. In this example $\ell = 1.5a$ and $d = 0.01\ell$.

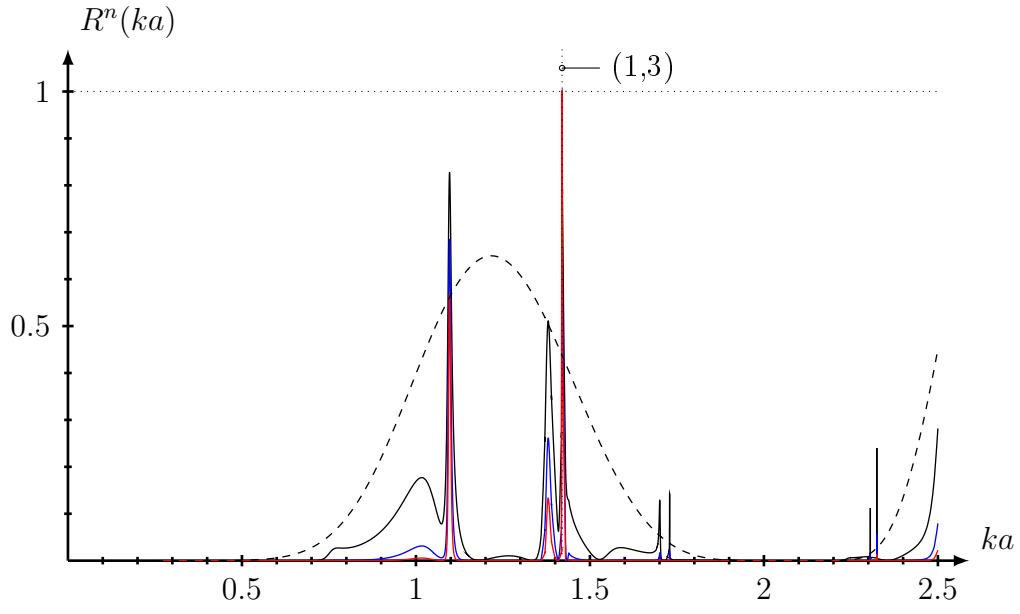

Figure 9: The same data as in Figure 8 but with unequalized data. The dashed curve shows the frequency taper of the antenna that is multiplied to the scattering data. The value is normalized with maximum absolute value of R in the interval.

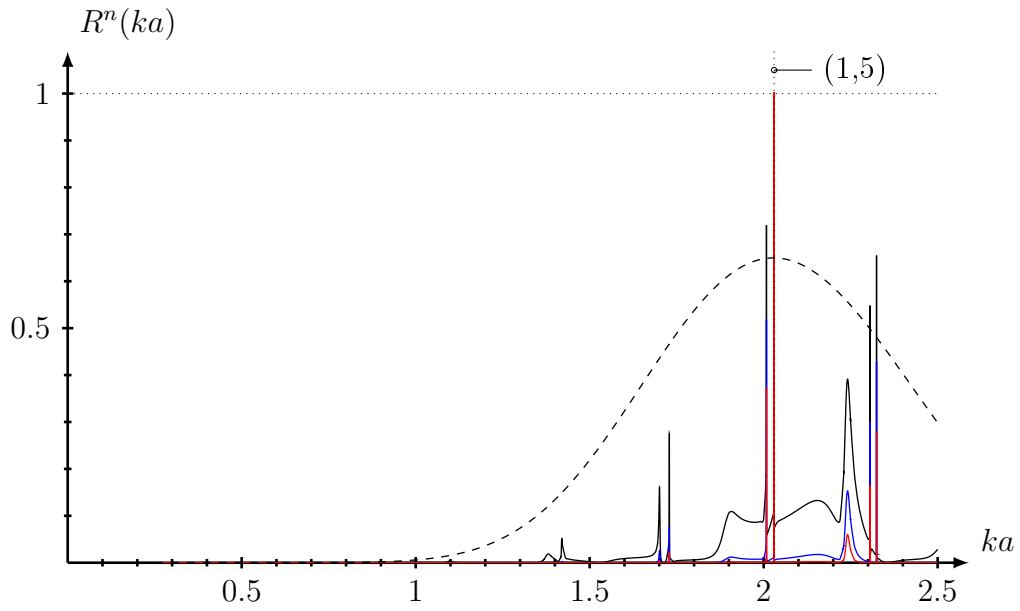

Figure 10: The value of the unequalized R^n for $n = 1, 2, 3$ for a single cylindrical dipole antenna with data $\ell = 0.9a$ and $d = 0.01\ell$. The value is normalized with maximum absolute value of R in the interval. The equalized case is identical to the curves in Figure 8. The dashed curve shows the frequency taper due to the antenna that is multiplied to the scattering data. The position of the largest resonance in the transition matrix is shown by a dotted vertical line.

different resonances are amplified. In particular, for the longer antenna configuration in Figure 11, the unequalized case amplifies the minor resonance (1,2), while the equalized case amplifies the main resonance (1,5). In Figure 12, the antennas are smaller: $\ell = 0.9a$, $d = 0.01\ell$, $\delta = 90°$, and $\theta = 30°$, and both the unequalized and the equalized iterations amplify the main (1,5) resonance. We conclude that properties of the illumination is important for the result.

6 Conclusions

We have shown, for realistic target and antenna models, that the iterative REM procedure can provide information about target resonances. We have shown that the process converges to the resonances of the overall antenna-target system, and we have proposed some approaches for removing the antenna response and range effects when these are known. We have shown that different antenna responses can result in different target resonances being identified.

We note that because the process uses data that is sampled in the time domain, the REM process converges automatically even to very narrow frequency-domain peaks. The only sampling issue that arises is in plotting the frequency-domain response.

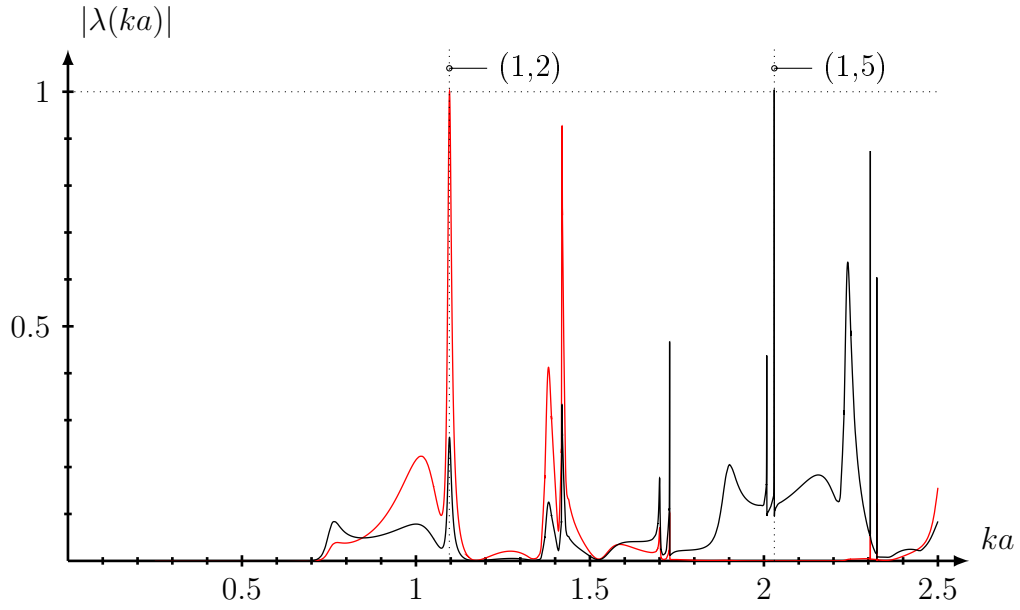

Figure 11: The largest eigenvalue $\lambda(ka)$ of $\mathbf{R}$ (red curve) and $\mathbf{R}_{\text{eq}}$ (black curve) for two identical cylindrical dipole antennas in Figure 5. The value is normalized with maximum absolute value of $\lambda_{\max}$ in the interval. The position of the corresponding pole in the transition matrix is shown by a dashed vertical line. In this example $\ell = 1.5a$, $d = 0.01\ell$, $\delta = 90°$, and $\theta = 30°$.

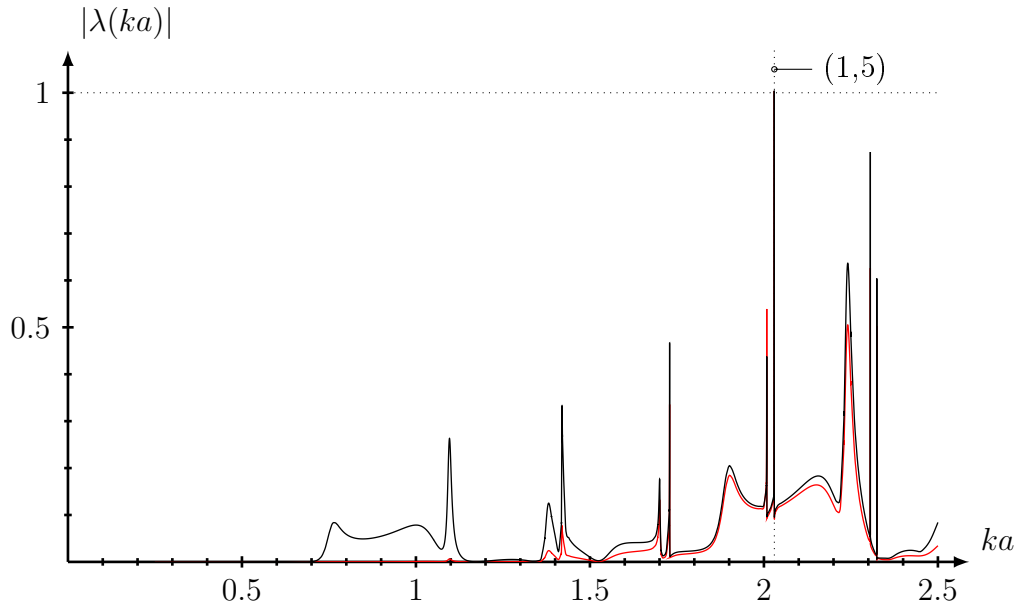

Figure 12: The same data as in Figure 11, but the excitation is made with a shorter antenna $\ell = 0.9a$.

A variety of interesting questions are left for the future.

- One of the advantages of REM over simply measuring the broadband response once and raising it to a power is the improvement in the signal-to-noise ratio of the resonance response. How much additive noise [20, 28] can REM accommodate?
- How does the REM process perform in the presence of interference?
- Can we use time-gating to identify resonances of a buried target?
- Is it possible to include a constraint that the transmitted waveform should have constant amplitude, and if so, does the modified process still provide target resonances?
- How can we best use the information provided by REM for target classification?
- How much extra information can be obtained from the use of polarization diversity?
- How can we use the REM process to identify the SEM poles in a stable way? The issue of extracting the SEM poles we take up in a subsequent paper.

Appendix A Spherical vector waves

The vector spherical harmonics are defined as [5, 29]

$$\begin{cases} \boldsymbol{A}_{1n}(\hat{\boldsymbol{r}}) = \dfrac{1}{\sqrt{l(l+1)}}\nabla\times(\boldsymbol{r}\mathrm{Y}_n(\hat{\boldsymbol{r}})) = \dfrac{1}{\sqrt{l(l+1)}}\nabla\mathrm{Y}_n(\hat{\boldsymbol{r}})\times\boldsymbol{r} \\ \boldsymbol{A}_{2n}(\hat{\boldsymbol{r}}) = \dfrac{1}{\sqrt{l(l+1)}}r\nabla\mathrm{Y}_n(\hat{\boldsymbol{r}}) \\ \boldsymbol{A}_{3n}(\hat{\boldsymbol{r}}) = \hat{\boldsymbol{r}}\mathrm{Y}_n(\hat{\boldsymbol{r}}), \end{cases}$$

where the spherical harmonics are denoted by $\mathrm{Y}_n(\hat{\boldsymbol{r}})$ defined as

$$\mathrm{Y}_n(\hat{\boldsymbol{r}}) = \mathrm{Y}_n(\theta,\phi) = \sqrt{\frac{\varepsilon_m}{2\pi}}\sqrt{\frac{2l+1}{2}\frac{(l-m)!}{(l+m)!}}\mathrm{P}_l^m(\cos\theta)\begin{Bmatrix}\cos m\phi \\ \sin m\phi\end{Bmatrix},$$

where $\mathrm{P}_l^m(x)$ are the associated Legendre functions, and where the Neumann factor is defined as

$$\varepsilon_m = 2-\delta_{m0},\ \textit{i.e.},\ \begin{cases}\varepsilon_0 = 1 \\ \varepsilon_m = 2, \quad m>0.\end{cases}$$

The index n is a multi-index for the integer indices $l = 1, 2, 3, \ldots$, $m = 0, 1, \ldots, l$, and $\sigma =$ e,o (even and odd in the azimuthal angle).[3] From these definitions we see

[3]The index set at several places in this paper also denotes a four index set, and includes the τ index. That is, the index n can denote $n = \{\sigma, l, m\}$ or $n = \{\tau, \sigma, l, m\}$.

that the first two vector spherical harmonics, $\boldsymbol{A}_{1n}(\hat{\boldsymbol{r}})$ and $\boldsymbol{A}_{2n}(\hat{\boldsymbol{r}})$, are tangential to the unit sphere Ω in $\mathbb{R}^3$ and they are related as

$$\begin{cases} \hat{\boldsymbol{r}} \times \boldsymbol{A}_{1n}(\hat{\boldsymbol{r}}) = \boldsymbol{A}_{2n}(\hat{\boldsymbol{r}}) \\ \hat{\boldsymbol{r}} \times \boldsymbol{A}_{2n}(\hat{\boldsymbol{r}}) = -\boldsymbol{A}_{1n}(\hat{\boldsymbol{r}}). \end{cases}$$

The vector spherical harmonics form an orthonormal set over the unit sphere Ω in $\mathbb{R}^3$, *i.e.*,

$$\iint_{\Omega} \boldsymbol{A}_{\tau n}(\hat{\boldsymbol{r}}) \cdot \boldsymbol{A}_{\tau' n'}(\hat{\boldsymbol{r}}) \, \mathrm{d}\Omega = \delta_{nn'}\delta_{\tau\tau'},$$

where $\mathrm{d}\Omega$ is the surface measure on the unit sphere.

The parity of the vector spherical harmonics is

$$\boldsymbol{A}_{\tau n}(-\hat{\boldsymbol{r}}) = (-1)^{l+\tau+1}\boldsymbol{A}_{\tau n}(\hat{\boldsymbol{r}}), \quad \tau = 1, 2. \tag{A.1}$$

The radiating solutions to the Maxwell equations in a homogeneous, isotropic media are defined as (outgoing spherical vector waves)

$$\begin{cases} \boldsymbol{u}_{1n}(k\boldsymbol{r}) = \dfrac{\xi_l(kr)}{kr}\boldsymbol{A}_{1n}(\hat{\boldsymbol{r}}) \\ \boldsymbol{u}_{2n}(k\boldsymbol{r}) = \dfrac{1}{k}\nabla \times \left(\dfrac{\xi_l(kr)}{kr}\boldsymbol{A}_{1n}(\hat{\boldsymbol{r}}) \right) \end{cases}$$

Here, we use the Riccati-Bessel functions $\xi_l(x) = x\mathrm{h}_l^{(1)}(x)$, where $\mathrm{h}_l^{(1)}(x)$ is the spherical Hankel function of the first kind [31]. These vector waves satisfy

$$\nabla \times (\nabla \times \boldsymbol{u}_{\tau n}(k\boldsymbol{r})) - k^2\boldsymbol{u}_{\tau n}(k\boldsymbol{r}) = \boldsymbol{0}, \qquad \tau = 1, 2$$

and they also satisfy the Silver-Müller radiation condition [13]. Another representation of the definition of the vector waves is

$$\begin{cases} \boldsymbol{u}_{1n}(k\boldsymbol{r}) = \dfrac{\xi_l(kr)}{kr}\boldsymbol{A}_{1n}(\hat{\boldsymbol{r}}) \\ \boldsymbol{u}_{2n}(k\boldsymbol{r}) = \dfrac{\xi_l'(kr)}{kr}\boldsymbol{A}_{2n}(\hat{\boldsymbol{r}}) + \sqrt{l(l+1)}\dfrac{\xi_l(kr)}{(kr)^2}\boldsymbol{A}_{3n}(\hat{\boldsymbol{r}}). \end{cases}$$

A simple consequence of these definitions is

$$\begin{cases} \boldsymbol{u}_{1n}(k\boldsymbol{r}) = \dfrac{1}{k}\nabla \times \boldsymbol{u}_{2n}(k\boldsymbol{r}) \\ \boldsymbol{u}_{2n}(k\boldsymbol{r}) = \dfrac{1}{k}\nabla \times \boldsymbol{u}_{1n}(k\boldsymbol{r}). \end{cases}$$

In a similar way, the regular spherical vector waves $\boldsymbol{v}_{\tau n}(k\boldsymbol{r})$ are defined [5].

$$\begin{cases} \boldsymbol{v}_{1n}(k\boldsymbol{r}) = \dfrac{\psi_l(kr)}{kr}\boldsymbol{A}_{1n}(\hat{\boldsymbol{r}}) \\ \boldsymbol{v}_{2n}(k\boldsymbol{r}) = \dfrac{\psi_l'(kr)}{kr}\boldsymbol{A}_{2n}(\hat{\boldsymbol{r}}) + \sqrt{l(l+1)}\dfrac{\psi_l(kr)}{(kr)^2}\boldsymbol{A}_{3n}(\hat{\boldsymbol{r}}) \end{cases}$$

where the ψ_l are the Riccati-Bessel functions $\psi_l(x) = x\mathrm{j}_l(x)$, and where $\mathrm{j}_l(x)$ is the spherical Bessel function [31].

Appendix B Resonances and poles of the transition matrix entries

The connection between the singularities of the transition matrix $t_{\tau l}$ and the peaks in the differential scattering cross section in the backward direction, $\sigma_{\rm b}(ka) = \frac{{\rm d}\sigma}{{\rm d}\Omega}(k, -\hat{\boldsymbol{k}}_{\rm i}, \hat{\boldsymbol{k}}_{\rm i})/\pi a^2$, is described in the literature, see *e.g.*, Reference 37. In this appendix, we review some of the details.

Denote the location of a pole in a transition matrix entry by $z_0 = x_0 - {\rm i}y_0$, where $y_0 > 0$, and denote for simplicity $ka = x \in \mathbb{R}$. In a neighborhood of the pole on the real axis, the transition matrix entry has the form

$$t_{\tau l}(x) = \frac{t_{\rm bg}(x)}{x - z_0},$$

where the background transition matrix $t_{\rm bg}(x)$ is a slowly varying analytic function. On the real axis, close to the pole z_0, the differential scattering cross section in the backward direction $\sigma_{\rm b}(x)$ has the form

$$\sigma_{\rm b}(x) = \frac{1}{x^2}\left| s_{\rm bg}(x) \pm (2l+1)\frac{t_{\rm bg}(x)}{x - z_0}\right|^2 = \frac{\sigma_{\rm bg}(x)}{|x - z_0|^2} = \frac{\sigma_{\rm bg}(x)}{(x-x_0)^2 + y_0^2}$$

where $s_{\rm bg}(x)$ and $\sigma_{\rm bg}(x)$ (background contribution) are smooth functions in the neighborhood of x_0. The maximum of the differential scattering cross section occurs at $x = x_m$, determined by

$$\left((x_m - x_0)^2 + y_0^2\right)\sigma'_{\rm bg}(x_m) - 2\sigma_{\rm bg}(x_m)\,(x_m - x_0) = 0, \tag{B.1}$$

where prime denotes differentiation w.r.t. x. If $\sigma'_{\rm bg}(x_m) = 0$ (constant background), then we conclude the maximum occurs at $x_m = x_0$.

If $\sigma'_{\rm bg}(x_m) \neq 0$, then the maximum is slightly shifted away from x_0. To proceed, it is convenient to introduce $f(x) = \sqrt{\sigma_{\rm bg}(x)} > 0$ (note that $\sigma_{\rm bg}(x) > 0$ in a neighborhood of $x = x_0$). Then (B.1) can be written

$$\left((x_m - x_0)^2 + y_0^2\right) f'(x_m) = f(x_m)\,(x_m - x_0)\,.$$

This root $x = x_m$ satisfies the approximate equation (use a linear approximation $f(x) \approx f(x_0) + f'(x_0)\,(x - x_0)$)

$$\left((x_m - x_0)^2 + y_0^2\right) f'(x_0) \approx \left(f(x_0) + f'(x_0)\,(x_m - x_0)\right)(x_m - x_0)\,,$$

with solution

$$x_m \approx x_0 + y_0^2\frac{f'(x_0)}{f(x_0)},$$

which quantifies the small shift of the resonance due to non-constant background, *i.e.*, $\sigma'_{\rm bg}(x_0) \approx \sigma'_{\rm bg}(x_m) \neq 0$. Note that a decrease in the value of y_0^2, decreases the shift.

Appendix C Energy and power flow

The received and transmitted power at time t are

$$P_{\mathrm{r}}(t) = \frac{|\boldsymbol{\beta}(t)|^2}{Z}, \qquad P_{\mathrm{t}}(t) = \frac{|\boldsymbol{\alpha}(t)|^2}{Z}$$

respectively, and the total energy received and transmitted are (Parseval's theorem is used)

$$E_{\mathrm{r}} = \frac{1}{\pi}\int_0^\infty \frac{|\boldsymbol{\beta}(k)|^2}{Z}\,\mathrm{d}\omega, \qquad E_{\mathrm{t}} = \frac{1}{\pi}\int_0^\infty \frac{|\boldsymbol{\alpha}(k)|^2}{Z}\,\mathrm{d}\omega$$

We observe that the power densities of the transmitted and received signals are $|\boldsymbol{\alpha}(k)|^2/Z$ and $|\boldsymbol{\beta}(k)|^2/Z$, respectively.

If we transmit the spatially distributed waveform determined by $\boldsymbol{\alpha}(k)$, which scatters from the target and results in the spatially distributed signal corresponding to $\boldsymbol{\beta}(k)$ on the receiving antennas, then our ability to detect the presence of the target is determined by the ratio $E_{\mathrm{r}}/E_{\mathrm{t}}$. The optimal detectability [10] is thus

$$\sup_{\boldsymbol{\alpha}} \frac{E_{\mathrm{r}}}{E_{\mathrm{t}}} = \sup_{\boldsymbol{\alpha}} \frac{\int_0^\infty \frac{|\boldsymbol{\beta}(k)|^2}{Z}\,\mathrm{d}\omega}{\int_0^\infty \frac{|\boldsymbol{\alpha}(k)|^2}{Z}\,\mathrm{d}\omega}.$$

Discussion of the effect of noise on the power method can be found in [20].

Appendix Acknowledgments

We would like to thank Ivars Kirsteins for helpful comments and discussions. The work of M.C. was supported in part by the Air Force Office of Scientific Research[4] under contract numbers FA9550-14-1-0185 and FA9550-18-1-0087.

References

[1] M. Abramowitz and I. A. Stegun, editors. *Handbook of Mathematical Functions.* Applied Mathematics Series No. 55. National Bureau of Standards, Washington DC, 1970.

[2] C. E. Baum. On the singularity expansion method for the solution of electromagnetic interaction problems. Technical report, Air Force Weapons Lab, Kirtland AFB, 12 1971.

[3] C. E. Baum. The singularity expansion method. In *Transient electromagnetic fields*, pages 129–179. Springer-Verlag, 1976.

[4] Consequently, the US Government is authorized to reproduce and distribute reprints for governmental purposes notwithstanding any copyright notation thereon. The views and conclusions contained herein are those of the authors and should not be interpreted as necessarily representing the official policies or endorsements, either expressed or implied, of the Air Force Research Laboratory or the US Government.

[4] B. Bogert. Demonstration of delay distortion correction by time-reversal techniques. *IRE Transactions on Communications Systems*, **5**(3), 2–7, December 1957.

[5] A. Boström, G. Kristensson, and S. Ström. Transformation properties of plane, spherical and cylindrical scalar and vector wave functions. In V. V. Varadan, A. Lakhtakia, and V. K. Varadan, editors, *Field Representations and Introduction to Scattering*, Acoustic, Electromagnetic and Elastic Wave Scattering, chapter 4, pages 165–210. Elsevier Science Publishers, Amsterdam, 1991.

[6] D. H. Chambers. Analysis of the time-reversal operator for scatterers of finite size. *J. Acoust. Soc. Am.*, **112**(2), 411–419, 2002.

[7] D. H. Chambers and J. G. Berryman. Analysis of the time-reversal operator for a small spherical scatterer in an electromagnetic field. *IEEE Trans. Antennas Propag.*, **52**(7), 1729–1738, 2004.

[8] D. H. Chambers and J. G. Berryman. Target characterization using decomposition of the time-reversal operator: electromagnetic scattering from small ellipsoids. *Inverse Problems*, **22**(6), 2145–2163, 2006.

[9] D. H. Chambers and A. K. Gautesen. Time reversal for a single spherical scatterer. *J. Acoust. Soc. Am.*, **109**(6), 2616–2624, 2001.

[10] M. Cheney and G. Kristensson. Optimal electromagnetic measurements. *J. Electromagnet. Waves Appl.*, **15**(10), 1323–1336, 2001.

[11] R. E. Collin. The receiving antenna. In R. E. Collin and F. J. Zucker, editors, *Antenna theory, part 1*, pages 93–137. McGraw-Hill, New York, NY, 1969.

[12] R. E. Collin. *Antennas and Radiowave Propagation.* McGraw-Hill, New York, NY, 1985.

[13] D. Colton and R. Kress. *Integral Equation Methods in Scattering Theory.* John Wiley & Sons, New York, NY, 1983.

[14] C. Dolph and S. Cho. On the relationship between the singularity expansion method and the mathematical theory of scattering. *IEEE Trans. Antennas Propag.*, **28**(6), 888–897, November 1980.

[15] R. S. Elliott. *Antenna Theory and Design.* IEEE Press, New York, NY, 2003. Revised edition.

[16] M. Fink and C. Prada. Acoustic time-reversal mirrors. *Inverse Problems*, **17**(1), R1, 2001.

[17] R. B. Green. *The general theory of antenna scattering.* PhD thesis, The Ohio State University, 1963.

[18] R. C. Hansen. Relationships between the antennas as scatterers and as radiators. *Proc. IEEE*, **77**, 659–662, 1989.

[19] V. G. Hansen. A sequential logic for improving signal detectability in frequency-agile search radars. *IEEE Transactions on Aerospace and Electronic Systems*, **AES-4**(5), 763–773, Sept 1968.

[20] M. Hardt and E. Price. The noisy power method: A meta algorithm with applications. In Z. Ghahramani, M. Welling, C. Cortes, N. D. Lawrence, and K. Q. Weinberger, editors, *Advances in Neural Information Processing Systems 27*, pages 2861–2869. Curran Associates, Inc., 2014.

[21] R. F. Harrington. Theory of loaded scatterers. *IEE Proceedings*, **111**, 617–623, 1964.

[22] D. Isaacson, M. Cheney, and M. Lassas. Optimal acoustic measurements. *SIAM J. Appl. Math.*, **61**(5), 1628–1647, 2001.

[23] L. B. Jackson. FIR filter design techniques. In *Digital Filters and Signal Processing*, pages 289–321. Springer, 1996.

[24] E. C. Jordan and K. G. Balmain. *Electromagnetic Waves and Radiating Systems.* Prentice-Hall, Inc., Englewood Cliffs, New Jersey, 1968.

[25] E. Kennaugh. The K-pulse concept. *IEEE Trans. Antennas Propag.*, **29**(2), 327–331, Mar 1981.

[26] J. Kim, M. Cheney, and E. Mokole. Tuning to resonances with iterative time reversal. *IEEE Trans. Antennas Propag.*, **64**(10), 4343–4354, Oct 2016.

[27] R. King and C. Harrison. The receiving antenna. *Proc. IRE*, **32**(1), 18–34, 1944.

[28] I. Kirsteins, A. Tesei, and J. Sessarego. Study of robustness of single-element-mirror time reversal method to reverberation and clutter: Simulations and tank measurements. *Proc. of the Underwater Acoustic Measurements: Technologies and Exhibition conference, Nafplion, Greece*, pages 349–356, 2009.

[29] G. Kristensson. *Scattering of Electromagnetic Waves by Obstacles.* Mario Boella Series on Electromagnetism in Information and Communication. SciTech Publishing, Edison, NJ, USA, 2016.

[30] L. Marin. Natural-mode representation of transient scattered fields. *IEEE Trans. Antennas Propag.*, **21**(6), 809–818, Nov 1973.

[31] F. W. J. Olver, D. W. Lozier, R. F. Boisvert, and C. W. Clark. *NIST Handbook of mathematical functions.* Cambridge University Press, New York, 2010.

[32] L. Pearson. Present thinking on the use of the singularity expansion in electromagnetic scattering computation. *Wave Motion*, **5**, 355–368, 1983.

[33] G. H. Price. On the relationship between the transmitting and receiving properties of an antenna. *IEEE Trans. Antennas Propag.*, **34**(11), 1366–1368, 1986.

[34] T. K. Sarkar and O. Pereira. Using the Matrix Pencil Method to Estimate the Parameters of a Sum of Complex Exponentials. *IEEE Antennas Propag. Mag.*, **37**(1), 48–55, 1995.

[35] T. K. Sarkar, S. Park, J. Koh, and S. M. Rao. Application of the Matrix Pencil Method for Estimating the SEM (Singularity Expansion Method) Poles of Source-Free Transient Responses from Multiple Look Directions. *IEEE Trans. Antennas Propag.*, **48**(4), 612–618, 2000.

[36] W. L. Stutzman and G. A. Thiele. *Antenna Theory and Design.* John Wiley & Sons, New York, NY, second edition, 1998.

[37] J. R. Taylor. *Scattering theory: the quantum theory of nonrelativistic collisions.* Robert E. Krieger Publishing Company, Malabar, Florida, 1983.

[38] H. Tortel, G. Micolau, and M. Saillard. Decomposition of the time reversal operator for electromagnetic scattering. *J. Electromagnet. Waves Appl.*, **13**(5), 687–719, 1999.

[39] Y. Ying-Zi, M. Li, and G. Sheng-Ming. Adaptive and optimal detection of elastic object scattering with single-channel monostatic iterative time reversal. *Chin. Phys. B*, **20**(5), 054301, 2011.